Chapter 4
Dynamic Analysis of a Pavement Structure Under a Vehicle's Moving Load

With the development of highway transportation, the high speed and heavy duty phenomena have become extraordinarily common. The premature pavement damage caused by the dynamic loads of heavy duty vehicles is becoming more and more serious and is receiving widespread attentions. The static highway design method has met difficulty to meet the traffic requirement. It is a prevailing subject to study the dynamics of pavement structure, to reveal the pavement damage mechanism, and to promote the changing of pavement design criterion from static to dynamic.

This chapter establishes the models of a finite (Sect. 4.1–4.3) and infinite beam (Sect. 4.4) on a nonlinear foundation with viscous damping. Based on the Galerkin method and the integral transform method, the numerical and analytical solutions are derived for the dynamic response of the pavement structure subjected to a moving load. Moreover, the vibration characteristics of the pavement structure under a moving load are discussed through some examples. Furthermore, the coupled nonlinear vibration of the vehicle–pavement system is studied based on a finite Timoshenko beam on the foundation subjected to a spring–mass–damper oscillator.

4.1 The Dynamic Response of a Vehicle–Pavement System Based on a Finite Beam on a Nonlinear Foundation

The dynamic response problem of elastic beams on a nonlinear viscoelastic foundation displays nonlinear and viscous characteristics, which make the analysis difficult. The Galerkin truncation method is a powerful tool for dealing with dynamic problems in such cases. It has been widely used to study free and forced vibration phenomena for elastic materials on nonlinear viscoelastic foundations. Based on the Galerkin method, Li et al. investigated the chaos of a pavement on a viscoelastic foundation subjected to a moving vehicle with the first order discretization and Melnikov's function [1]; Sheng et al. studied the dynamic behavior of Timoshenko beams with damage on a viscoelastic foundation by using 2-term truncation [2];

S. Yang et al., *Dynamics of Vehicle-Road Coupled System,*
DOI 10.1007/978-3-662-45957-7_4

Pellicano and Mastroddi investigated the nonlinear dynamic behavior via 3-term truncation in conjunction with the method of normal forms [3]; Ansari et al. studied train–track interaction via 3-term truncation, considering the internal–external resonance condition and obtained the frequency responses of different harmonics, and found that the nonlinear stiffness plays a positive role in the design of railway tracks because of the delay in the jump phenomenon [4, 5]; Yan et al. studied the dynamic response of functionally graded beams with an open edge crack on an elastic foundation subjected to a transverse moving load via 3-term truncation [6]; Coskun studied the forced vibrations of an elastic beam on a nonlinear tensionless foundation by employing the 5-term truncation [7]; Celep et al. investigated the response of a beam on a tensionless Pasternak foundation subjected to a dynamic load by employing the 5-term truncation [8]; Vassilev and Djondjorov investigated the dynamic stability of viscoelastic pipes lying on a foundation of variable modulus using 10-term truncation [9]; Yang et al. presented the dynamic behavior of the vehicle–pavement-foundation coupled system using the 20-term truncation [10]; Chen and Chen studied steady-state deformations of an infinite beam on a tensionless foundation under a moving point load through 80-term truncation [11]; Senalp et al. studied the dynamic response of a finite length Euler–Bernoulli beam on linear and nonlinear viscoelastic foundations under a concentrated moving force, and 100-term truncation is utilized in order to solve the governing equations of motion [12].

Although the Galerkin truncation has been widely applied to dynamic problems of finite beams on a nonlinear viscoelastic foundation, the convergence of the truncation terms has not been studied. In this section, the convergence of Galerkin's method for dynamic response of finite Euler–Bernoulli beams on a cubic nonlinear foundation with viscous damping is studied. The parametric dependence study is carried out to investigate the effects of different parameters on the convergence of the Galerkin truncation.

The dynamic response of a finite beam on an elastic foundation has been studied through different boundary conditions. Based on the finite element method for the dynamic analysis of beams on an elastic foundation subjected to moving point loads, Thambiratnam and Zhuge proved that the beams of span length $L > 10$ m can accurately approximate the response of the ideal beam of infinite length [13]. In order to study the interaction between train vehicles and railway track, Muscolino and Palmeri scrutinized the response of beams on a viscoelastic foundation under moving single degree-of-freedom (SDOF) oscillators [14]. Based on modal shapes and natural frequencies of the beam-foundation, the effects of boundary conditions and the span length of the beam are investigated through a state–space formulation. Monsalve et al. presented the dynamic analysis of a Timoshenko beam-column on a two-parameter elastic foundation with generalized end conditions. The end conditions allowed simulating any end support condition to the beam-column [15]. The dynamic responses of functionally graded beams on an elastic foundation subjected to a moving load with different end supports are obtained by Yan et al. [6]. The authors found that boundary conditions have significant influence on the dynamic response of the cracked functionally graded materials' beams. However, there are no works on the influences of boundary conditions of finite beams on a foundation on

the dynamic response of the beams excited by a moving load and the convergence of the Galerkin's method. To address the lack of research in this aspect, the dynamic responses are calculated by the Galerkin truncation under three types of the conventional boundary conditions, namely simply-supported (SS), clamped–clamped (CC), and free–free (FF) boundary conditions. In the present work, the effects of the boundary condition and span length of the supporting beam on the dynamic responses and the convergence of the Galerkin truncation are studied.

This section investigates the convergence of Galerkin's method for the dynamic response of a vehicle–pavement system. The pavement is modeled as a finite length Euler–Bernoulli or a Timoshenko beam with uniform cross-section on a nonlinear viscoelastic foundation. The vehicle is simplified as a concentrated force or a spring–mass–damper oscillator. Galerkin's method is utilized to discretize the nonlinear partial differential governing equation of the forced vibration. Moreover, the dependence of the convergence of Galerkin's method on boundary conditions, span length, and other system parameters is studied, respectively.

4.1.1 Equation of Motion [16]

The system under investigation is a finite elastic Euler–Bernoulli beam on a nonlinear viscoelastic foundation and subjected to a moving load. Consider a homogeneous beam with constant cross-section A, moment of inertial I, length L, densityρ, and modulus of elasticity E. The foundation is taken as a nonlinear Winkler's foundation with liner-plus-cubic stiffness and viscous damping with three parameters as follows

$$P = k_1 w + k_3 w^3 + c w_{,T} \tag{4.1}$$

where P represents the force induced by the foundation per unit length of the beam, k_1 and k_3 are the linear and nonlinear foundation parameters, respectively, μ is the damping coefficient of the foundation, T is the time, a comma preceding T denotes the partial differentiation with respect to T.

Using the Hamilton principle and considering the Euler–Bernoulli beam theory, one can develop the governing differential equation of motion for the beam as

$$\rho A w_{,TT} + EI w_{,XXXX} + k_1 w + k_3 w^3 + c w_{,T} = F_z \delta(X - VT) \tag{4.2}$$

where $w(X, T)$ is the vertical displacement function, EI is the flexural rigidity of the beam, X is the spatial coordinate along the axis of the beam, $\delta(X)$ is the Dirac delta function used to deal with the moving concentrated load, a comma preceding X denotes the partial differentiation with respect to X, F_z and v are the magnitudes of the load and load speed, respectively.

Introduce the dimensionless variables and parameters as follows

$$w \leftrightarrow \frac{w}{L}, t = \frac{T}{L}\sqrt{\frac{E}{\rho}}, v = V\sqrt{\frac{\rho}{E}}, x = \frac{X}{L}, k_{\mathrm{b}} = \frac{1}{L}\sqrt{\frac{I}{A}},$$
$$F_z \leftrightarrow \frac{F_z}{EA}, c \leftrightarrow \frac{c}{A}\sqrt{\frac{L^2}{\rho E}}, k_1 \leftrightarrow \frac{k_1 L^2}{EA}, k_3 \leftrightarrow \frac{k_3 L^4}{EA} \tag{4.3}$$

where x is the dimensionless spatial coordinate and t is the dimensionless time. Equation (4.2) can be transformed into the dimensionless equation

$$w_{,tt} + k_{\mathrm{b}}^2 w_{,xxxx} + k_1 w + k_3 w^3 + c w_{,t} = F_z \delta(x - vt) \tag{4.4}$$

Here, the beam considered in the model, is assumed to be simply supported at both ends, and therefore the boundary conditions are given as follows

$$w(0,t) = w(1,t) = 0, w_{,xx}(0,t) = w_{,xx}(1,t) = 0 \tag{4.5}$$

In the present investigation, two other kinds of boundary conditions of the beam are also considered, that is, both clamped ends, as follows

$$w(0,t) = w(1,t) = 0, w_{,x}(0,t) = w_{,x}(1,t) = 0 \tag{4.6}$$

and both free ends as follows

$$w_{,xx}(0,t) = w_{,xx}(1,t) = 0, w_{,xxx}(0,t) = w_{,xxx}(1,t) = 0 \tag{4.7}$$

In all numerical examples here, the initial conditions are

$$w(x,t)\Big|_{t=0} = 0, \quad w_{,t}(x,t)\Big|_{t=0} = 0 \tag{4.8}$$

4.1.2 Galerkin's Discretization

The Galerkin truncation method is used to discretize the system and the series expansion form for $w(x, t)$ is assumed to be

$$w(x,t) = \sum_{k=1}^{\infty} q_k(t)\varphi_k(x) \tag{4.9}$$

where $\varphi_k(x)$ are the trial functions, and $q_k(t)$ are sets of generalized displacements of the beams. In this research, the first n terms of Eq. (4.9) is considered in order to determine $w(x, t)$. Substituting Eq. (4.9) into Eq. (4.4) leads to

$$\begin{aligned}&\sum_{k=1}^{n}\left\{\left[\ddot{q}_k(t)+k_1 q_k(t)+c\dot{q}_k(t)\right]\varphi_k(x)\right\}+k_b^2\sum_{k=1}^{n}\left[q_k(t)\varphi_k''''(x)\right]\\&+k_3\left\{\sum_{k=1}^{n}\left[q_k(t)\varphi_k(x)\right]\right\}^3-F_z\delta(x-vt)=0\end{aligned}\tag{4.10}$$

Multiplying Eq. (4.10) by the weight functions $w_i(x)$ and integrating it over the interval of 0 and 1, the Galerkin procedure leads to the following set of n second-order ordinary differential equations (ODES)

$$\begin{aligned}&\sum_{k=1}^{n}\left\{\left[\ddot{q}_k(t)+k_1 q_k(t)+c\dot{q}_k(t)\right]\int_0^1\varphi_k(x)w_i(x)\mathrm{d}x\right\}\\&+k_b^2\sum_{k=1}^{n}\left[q_k(t)\int_0^1\varphi_k''''(x)w_i(x)\mathrm{d}x\right]\\&+k_3\int_0^1\left\{\sum_{k=1}^{n}\left[q_k(t)\varphi_k(x)\right]\right\}^3 w_i(x)\mathrm{d}x-F_z w_i(vt)=0\\&i=1,2,...,n\end{aligned}\tag{4.11}$$

If the trial functions and the weight functions are both chosen properly, the vertical displacement of the beams $w_n(x,t)$ can be numerically solved via Eq. (4.9).

In the present investigation, both the trial and weight functions are chosen as eigenfunctions of the beam-foundation linear subsystem under the boundary conditions. The natural frequencies and the mode functions of the beam on a linear elastic foundation which is simply supported and without any loads can be derived as follows

$$\omega_k^2=k_b^2\beta_k^4+k_1,\ (k=1,2,\cdots)\tag{4.12}$$

and

$$\phi_k(x)=\sin(\beta_k x),(k=1,2,\cdots)\tag{4.13}$$

where

$$\beta_k=k\pi,(k=1,2,\cdots)\tag{4.14}$$

When the beam is CC at the ends, the kth mode functions is

$$\phi_k(x)=\cosh\beta_k x-\cos\beta_k x+\xi_k(\sin\beta_k x-\sinh\beta_k x),k=1,2,\ldots\tag{4.15}$$

where

$$\xi_k = \frac{\cosh \beta_k - \cos \beta_k}{\sinh \beta_k - \sin \beta_k}, (k = 1, 2, \cdots) \tag{4.16}$$

and the characteristic equation is

$$\cos \beta_k \cosh \beta_k = 1 \tag{4.17}$$

whose nontrivial solutions should be numerically computed: $\beta_1 = 4.73, \beta_2 = 7.85, \ldots$ (notice that $\beta_k \cong (2k+1)\pi/2$ for $k > 2$).

When the beam is FF at the ends, the kth mode functions is

$$\phi_k(x) = \cos \beta_k x + \cosh \beta_k x + \xi_k (\sin \beta_k x + \sinh \beta_k x), k = 1, 2, \cdots \tag{4.18}$$

where

$$\xi_k = -\frac{\cos \beta_k - \cosh \beta_k}{\sin \beta_k - \sinh \beta_k} = -\frac{\cos \beta_k + \cosh \beta_k}{\sin \beta_k + \sinh \beta_k}, k = 1, 2, \cdots \tag{4.19}$$

and the characteristic equation is Eq. (4.17), same as CC boundary conditions. The eigenvalues are $\beta_1 = 0, \beta_2 = 4.73, \beta_3 = 7.85 \ldots$ (notice that $\beta_k \cong (2k-1)\pi/2$ for $k > 3$).

Both the trial and weight functions are chosen as eigenfunctions of the beam-foundation linear subsystem. That is to say, $\varphi_k(x) = \phi_k(x)$, $w_i(x) = \phi_i(x)$. For SS, CC, and FF boundary conditions, the mode functions satisfied

$$\varphi_k'''' = \beta_k^4 \varphi_k(x) \tag{4.20}$$

With the usual orthogonal condition, the CC and FF boundary conditions satisfied

$$\int_0^1 \varphi_k(x) w_i(x) \mathrm{d}x = \begin{cases} 0, & k \neq i \\ 1, & k = i \end{cases} \tag{4.21}$$

Substitution of Eq. (4.21) into Eq. (4.11) yields

$$\begin{aligned} &\ddot{q}_i(t) + c\dot{q}_i(t) + \left(k_1 + k_\mathrm{b}^2 \beta_i^4\right) q_i(t) - F_z w_i(vt) \\ &+ k_3 \int_0^1 \left\{ \sum_{k=1}^{n} \left[q_k(t) \varphi_k(x) \right] \right\}^3 w_i(x) \mathrm{d}x = 0 \end{aligned} \tag{4.22}$$

For a set of given parameters k_b, k_1, k_3, F_z, μ and the initial conditions in Eq. (4.8), $q_k(t)$ can be numerically solved via the Runge–Kutta method (fourth order) from Eq. (4.22) by discretizing the temporal variables. After substituting the numerical solutions into Eq. (4.9), the vertical displacement $w_n(x,t)$ can be solved.

4.1.3 Numerical Results

In this part, the beam is assumed to be the asphalt mixtures D-12 (limestone). The physical and geometric properties and dimensionless parameters' value of the pavement, foundation, and the moving load are listed in Table 4.1.

The results of a few different numbers of Galerkin truncation terms, namely, 50-term Galerkin's truncation, 75-term Galerkin's truncation, 150-term Galerkin's truncation, and 200-term Galerkin's truncation for the vertical deflections of the asphalt pavement while the load moves to the mid-point of the pavement and the vertical deflections of pavement center with time are, respectively, shown in Figs. 4.1 and 4.2. The numerical results demonstrated that there are big differences between the 50-term Galerkin's truncation results with the 150-term ones and the 200-term ones. The comparisons indicate that the 50-term Galerkin's method is not accurate enough for the dynamic response analysis of the asphalt pavement on a soft soil foundation running the vehicle, and there are discernible differences between the results of the 75-term and the 150-term Galerkin's method. The comparisons also predict that the difference between the results of the 150-term and the 200-term Galerkin's method is very small, so the 150-term Galerkin's method yields rather accurate results. The maximum relative differences between the maximum mid-point vertical deflections is 14.29×10^{-2} in the 50-term Galerkin truncation and the 200-term Galerkin truncation, 4.876×10^{-2} in the 75-term Galerkin truncation and the 200-term Galerkin truncation, and 0.3381×10^{-2} in the 150-term Galerkin truncation and 200-term Galerkin truncation.

Table 4.1 Properties of the asphalt mixtures D-12, pavement, foundation, and load [17]. (Reprinted from ref. [16], Copyright 2014, with permission from Elsevier)

Item	Notation	Value	Dimensionless value
Asphalt mixtures (D–12)			
Young's modulus(steel)	E	6.998 GPa	–
Mass density	ρ	2373 kg/m^3	–
Height of pavement	h	0.3 m	–
Width of pavement	b	1.0 m	–
Modulus of elasticity	k_b	–	5.41×10^{-4}
Length	L	160 m	1
Foundation			
Mean stiffness	k_1	8×10^6 N/m^2	97.552
Nonlinear stiffness	k_3	8×10^6 N/m^4	2.497×10^6
Viscous damping	c	0.3×10^6 Ns/m^2	39.263
Moving load			
Load	F_z	212.6 KN	1.013×10^{-4}
Speed	V	20 m/s	0.01165

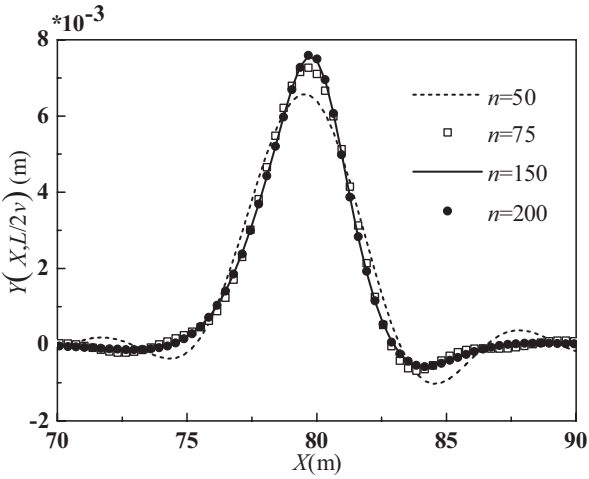

Fig. 4.1 The effects of the Galerkin truncation terms on the vertical deflection of the pavement. (Reprinted from ref. [16], Copyright 2014, with permission from Elsevier)

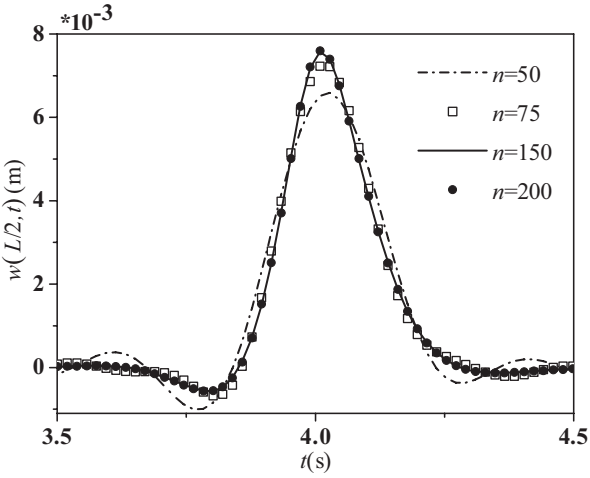

Fig. 4.2 The effects of the Galerkin truncation terms on the vertical displacements of the pavement's midpoint. (Reprinted from ref. [16], Copyright 2014, with permission from Elsevier)

In Figs. 4.3 and 4.4, the effects of three kinds of boundary conditions on the vertical displacements of the pavement midpoint ($X = L/2$) while $T = L/(2V)$ versus the truncation terms and the shape of the pavement while $T = L/(2V)$ are displayed. In Fig. 4.4a, the effects of three kinds of boundary conditions on the vertical displacements of the pavement midpoint ($X = L/2$) while $T = L/(2V)$ versus the truncation terms are displayed. Figure 4.4b shows the kth-order of the natural frequencies. The numerical results also illustrate that the convergence for simply supported boundary conditions is slightly slower, the same as changing tendencies of the natural frequencies. The numerical results which are shown in Fig. 4.4 also illustrate that the convergence can be predicted from the growth in the natural frequencies.

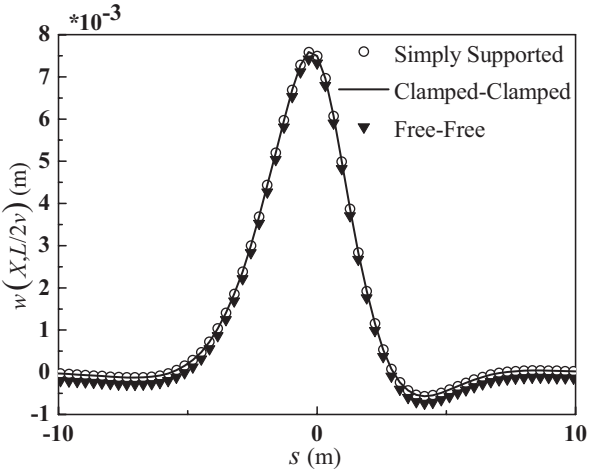

Fig. 4.3 The effects of the boundary conditions on the vertical deflection of the pavement: $n = 200$. (Reprinted from ref. [16], Copyright 2014, with permission from Elsevier)

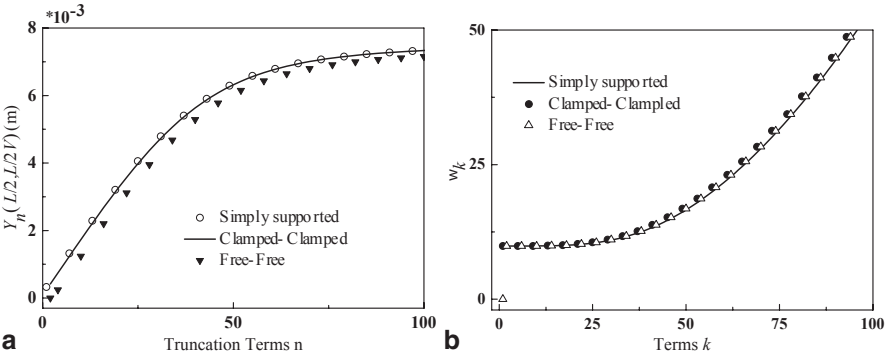

Fig. 4.4 The effects of the boundary conditions: **a** on the vertical displacements of the pavement midpoint versus truncation terms; **b** on the natural frequencies versus terms. (Reprinted from ref. [16], Copyright 2014, with permission from Elsevier)

In the following calculations for the asphalt pavement on a soft soil foundation with a moving vehicle, only the results of the simply supported boundary conditions are shown. Figure 4.5 shows the dependence of the convergence in terms of the vertical deflections of the pavement on the system parameters. There is a little difference among the vertical deflections for different lengths of the beam while the truncation terms are not too large, which means $n < 20$. The numerical results also illustrate that when a longer length of the pavement L is chosen, more truncation terms are required to achieve convergence. The convergence of Galerkin's method depends on the pavement and foundation parameters, including the modulus of elasticity of the pavement, height and width of the pavement, the linear and nonlinear foundation parameters, and the damping coefficient of the foundation, which are displayed in Fig. 4.5, respectively. The numerical results of the asphalt pavement

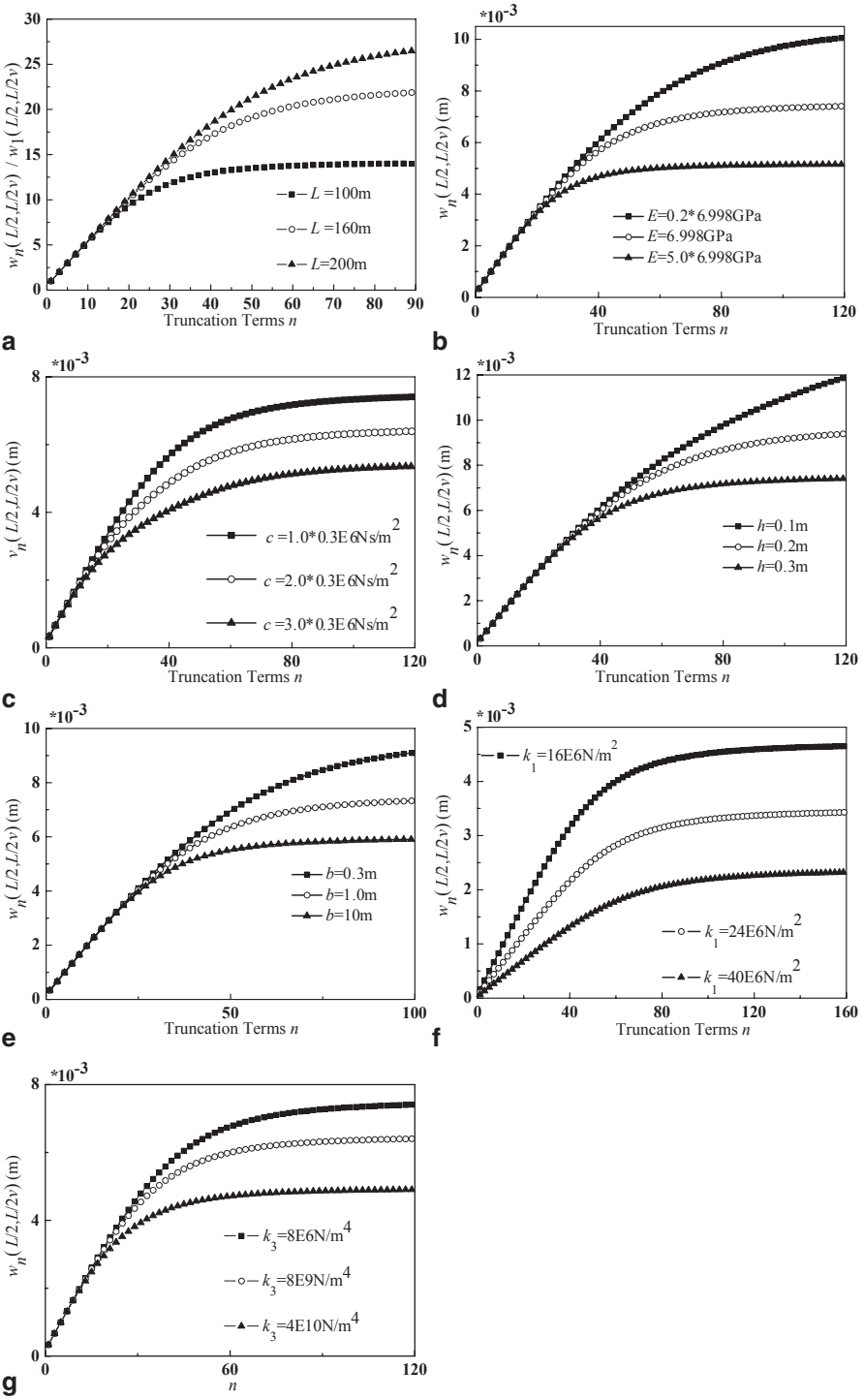

Fig. 4.5 The effects of the parameters on the vertical displacements of the pavement midpoint versus truncation terms. (Reprinted from ref. [16], Copyright 2014, with permission from Elsevier)

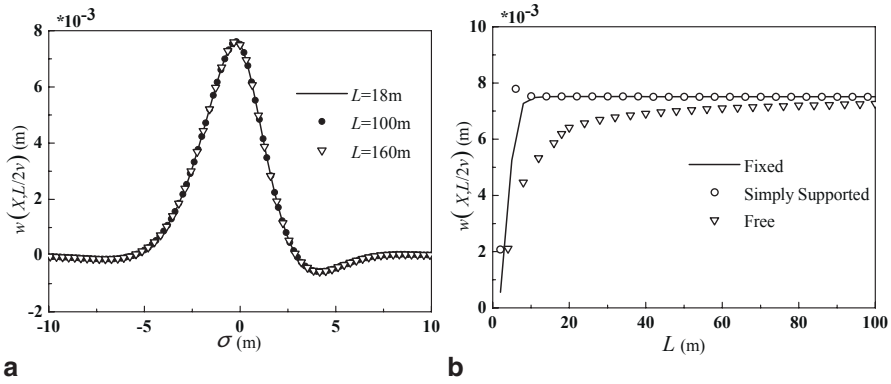

Fig. 4.6 The effects of the span length of the pavement on the vertical deflection of the pavement with $n=200$. (Reprinted from ref. [16], Copyright 2014, with permission from Elsevier)

on a soft soil foundation with a moving vehicle illustrate that the convergence of the Galerkin truncation increases with the growing modulus of elasticity of the pavement, the nonlinear foundation parameters, but decreases with the increase of the linear foundation parameters and the damping coefficient. It is also found that the convergence increases with the height and the width of the pavement. The numerical results also depict that there is a little difference among the vertical deflections of the pavement for not too large truncation terms with the different modulus of elasticity of the pavement, nonlinear foundation parameters, the height and the width of the beam, and the damping coefficient of the foundation. The vertical displacements of the pavement decrease with the increase of these parameters.

The vertical deflections of the asphalt pavement while the load moves to midpoint of the pavement for different lengths of pavement and different boundary conditions are shown in Fig. 4.6a and b, respectively. Figure 4.6a demonstrates that beams of span length $L=18\text{m}$ with SS or CC boundary conditions can accurately approximate the response of the infinite length asphalt pavement on a soft soil foundation with a moving vehicle, and three solutions are overlapped when the span length of the pavement is rather large. Figure 4.6b indicates that the FF boundary conditions are the inefficient ones.

4.2 The Dynamic Response of a Finite Timoshenko Beam on a Nonlinear Viscoelastic Foundation to a Moving Load [18]

4.2.1 Equation of Motion

The system under investigation is a finite elastic Timoshenko beam on a nonlinear viscoelastic foundation subjected to a moving load, as shown in Fig. 4.7. F_0 and V, respectively, represent the magnitude of the load and the load speed. Moreover, V

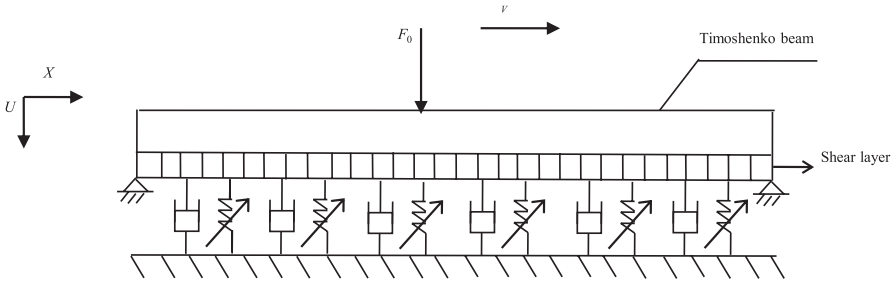

Fig. 4.7 The model of a finite Timoshenko beam on a nonlinear viscoelastic Pasternak foundation. (Reprinted from ref. [18], with kind permission from Springer Science+Business Media)

is assumed to be constant. X and U are the spatial coordinate along the axis of the beam and the vertical displacement function, respectively. Consider a homogeneous beam with constant cross-section A, moment of inertial I, length L, density ρ, modulus of elasticity E, shear modulus G, and effective shear area $k'A$.

The foundation is taken as a nonlinear Pasternak foundation with linear-plus-cubic stiffness and viscous damping as follows:

$$P(x,t) = k_1 U(X,T) + k_3 U^3(X,T) + \mu \frac{\partial U(X,T)}{\partial T} - G_p \frac{\partial^2 U(X,T)}{\partial X^2} \tag{4.23}$$

where P represents the force induced by the foundation per unit length of the beam. k_1 and k_3 are the linear and nonlinear foundation parameters, respectively. Furthermore, G_p and μ are the shear deformation coefficient and the damping coefficient of the foundation, respectively, and T is the time.

Using the Hamilton principle and considering the Timoshenko beam theory, one can develop the governing differential equations of motion for the beam as

$$\begin{aligned}
&\rho A \frac{\partial^2 U}{\partial T^2} + k'AG\left[\frac{\partial \psi}{\partial X} - \frac{\partial^2 U}{\partial X^2}\right] + k_1 U + k_3 U^3 + \mu \frac{\partial U}{\partial T} - G_p \frac{\partial^2 U}{\partial X^2} = F_0 \delta(X - VT), \\
&\rho I \frac{\partial^2 \psi}{\partial T^2} - EI \frac{\partial^2 \psi}{\partial X^2} + k'AG\left[\psi - \frac{\partial U}{\partial X}\right] + k_f \psi + c_f \frac{\partial \psi}{\partial T} = 0
\end{aligned} \tag{4.24}$$

where k_f and c_f are the foundation rocking stiffness and the damping coefficient, $\psi(X,T)$ is the slope function due to bending of the beam, $\delta(X - VT)$ is the Dirac delta function used to deal with the moving concentrated load.

Introduce the dimensionless variables and parameters as follows

$$\begin{aligned}
&u = \frac{U}{L}, t = \frac{T}{L}\sqrt{\frac{E}{\rho}}, x = \frac{X}{L}, \psi = \psi, v = V\sqrt{\frac{\rho}{E}}, \alpha = \frac{k'G}{E}, \beta = k'AG\frac{L^2}{EI}, k_1 \leftrightarrow \frac{k_1 L^2}{EA}, \\
&k_3 \leftrightarrow \frac{k_3 L^4}{EA}, \mu \leftrightarrow \frac{\mu}{A}\sqrt{\frac{L^2}{\rho E}}, G_p \leftrightarrow G_p \frac{1}{EA}, F_0 \leftrightarrow \frac{F_0}{EA}, k_f \leftrightarrow k_f \frac{L^2}{EI}, c_f \leftrightarrow \frac{c_f}{I}\sqrt{\frac{L^2}{\rho E}}
\end{aligned} \tag{4.25}$$

where x is the dimensionless spatial coordinate and t is the dimensionless time. Equation (4.24) can be transformed into the following dimensionless equation

$$\begin{aligned}&\frac{\partial^2 u}{\partial t^2}+\alpha\left[\frac{\partial \psi}{\partial x}-\frac{\partial^2 u}{\partial x^2}\right]+k_1 u+k_3 u^3+\mu\frac{\partial u}{\partial t}-G_{\mathrm{p}}\frac{\partial^2 u}{\partial x^2}=F_0\delta(x-vt),\\&\frac{\partial^2 \psi}{\partial t^2}-\frac{\partial^2 \psi}{\partial x^2}+\beta\left[\psi-\frac{\partial u}{\partial x}\right]+k_{\mathrm{f}}\psi+c_{\mathrm{f}}\frac{\partial \psi}{\partial t}=0\end{aligned} \tag{4.26}$$

4.2.2 Normal Modes

The harmonic solution can be assumed in the form

$$\begin{aligned}u(x,t)&=\sum_{k=1}^{\infty}\varphi_k(x)e^{\mathrm{i}\omega_k t},\\\psi(x,t)&=\sum_{k=1}^{\infty}\upsilon_k(x)e^{\mathrm{i}\omega_k t}\end{aligned} \tag{4.27}$$

where ω_k are the natural frequencies, and $\varphi_k(x)$ and $\upsilon_k(x)$ are the corresponding mode functions of the beam on a linear Pasternak foundation, which can be derived from Eq. (4.26) as follows

$$\begin{aligned}&\frac{\mathrm{d}^2\varphi_k}{\mathrm{d}x^2}+a\varphi_k-\frac{c}{\beta}\frac{\mathrm{d}\upsilon_k}{\mathrm{d}x}=0,\\&\frac{\mathrm{d}^2\upsilon_k}{\mathrm{d}x^2}+b\upsilon_k+\beta\frac{\mathrm{d}\varphi_k}{\mathrm{d}x}=0\end{aligned} \tag{4.28}$$

where

$$a=(\omega_k{}^2-k_1)/(\alpha+G_{\mathrm{p}}),b=\omega_k{}^2-\beta-k_{\mathrm{f}},c=\alpha\beta/(\alpha+G_{\mathrm{p}})$$

By eliminating the functions U_k from Eq. (4.28), one obtains the Timoshenko beam equations of free vibration in the form

$$\begin{aligned}&\frac{\mathrm{d}^4\varphi_k}{\mathrm{d}x^4}+p\frac{\mathrm{d}^2\varphi_k}{\mathrm{d}x^2}+q\varphi_k=0,\\&p=a+b+c,q=ab\end{aligned} \tag{4.29}$$

Thus the characteristic equation has the form

$$r^4+pr^2+q=0 \tag{4.30}$$

Replacing $z = r^2$ casts Eq. (4.30) in the form

$$z^2 + pz + q = 0 \tag{4.31}$$

Its roots are

$$z_1 = \frac{1}{2}(-p + \sqrt{\Delta}), z_2 = \frac{1}{2}(-p - \sqrt{\Delta}) \tag{4.32}$$

where $\Delta = (-c + a - b)^2 + 4ac$.

Now, one should discuss the sign of the roots z_1 and z_2: $\forall_{\omega k} \Leftrightarrow z_2 < 0; z_1 > 0$ for $q < 0$; $z_1 < 0$ for $q > 0$.

Two possible solutions to Eq. (4.28) can be obtained:

a. For $q < 0$,

$$\begin{aligned} \varphi(x) &= C_1 \cosh \lambda_1 x + C_2 \sinh \lambda_1 x + C_3 \cos \lambda_2 x + C_4 \sin \lambda_2 x, \\ \upsilon(x) &= C_1' \sinh \lambda_1 x + C_2' \cosh \lambda_1 x + C_3' \sin \lambda_2 x + C_4' \cos \lambda_2 x \end{aligned} \tag{4.33}$$

b. For $q > 0$,

$$\begin{aligned} \varphi(x) &= H_1 \cos \lambda_1 x + H_2 \sin \lambda_1 x + H_3 \cos \lambda_2 x + H_4 \sin \lambda_2 x, \\ \upsilon(x) &= H_1' \sin \lambda_1 x + H_2' \cos \lambda_1 x + H_3' \sin \lambda_2 x + H_4' \cos \lambda_2 x \end{aligned} \tag{4.34}$$

where the integration constants C_i, C_i', H_i, and H_i' depend on the boundary conditions.

The simply supported boundary condition analyzed in this research is the most frequently encountered boundary condition for the present problem. The boundary conditions for a simply supported beam are

$$\begin{aligned} &\varphi(0) = \varphi(1) = 0, \\ &\varphi''(0) + a\varphi(0) = \varphi''(1) + a\varphi(1) = 0 \end{aligned} \tag{4.35}$$

a. For $q < 0$, the solution to Eq. (4.29) has the form (4.33). From the boundary conditions at $x = 0$, the following equations are obtained

$$C_1 + C_3 = 0, \lambda_1^2 C_1 - \lambda_2^2 C_3 = 0 \tag{4.36}$$

The system of equations is satisfied when $C_1 = C_3 = 0$, which corresponds to the solution for the Euler–Bernoulli beam.

The boundary conditions at $x = 1$ are expressed by the matrix equation

$$\begin{bmatrix} \sinh \lambda_1 & \sinh \lambda_2 \\ \lambda_1^2 \sinh \lambda_1 & -\lambda_2^2 \sinh \lambda_2 \end{bmatrix} \begin{bmatrix} C_2 \\ C_4 \end{bmatrix} = \begin{bmatrix} 0 \\ 0 \end{bmatrix} \tag{4.37}$$

The nontrivial solution to Eq. (4.37) is obtained from the condition that the main matrix determinant is equal to zero. Thus, one can obtain the frequency equation

$$\sin \lambda_2 = 0 \tag{4.38}$$

Consequently, the corresponding *i*th normal modes with simply supported boundary conditions can be obtained as

$$\begin{aligned} \phi(x) &= C \sin \lambda_2 x, \\ \upsilon(x) &= C' \cos \lambda_2 x \end{aligned} \tag{4.39}$$

b. For $q > 0$, the solution to Eq. (4.29) has the form (4.34). From the boundary conditions at $x = 0$, the following equations are obtained

$$H_1 + H_3 = 0, \lambda_1^2 H_1 + \lambda_2^2 H_3 = 0 \tag{4.40}$$

The system of equations is satisfied when $H_1 = H_3 = 0$.

The boundary conditions at $x = 1$ are expressed by the matrix equation

$$\begin{bmatrix} \sin \lambda_1 & \sin \lambda_2 \\ -\lambda_1^2 \sin \lambda_1 & -\lambda_2^2 \sin \lambda_2 \end{bmatrix} \begin{bmatrix} H_2 \\ H_4 \end{bmatrix} = \begin{bmatrix} 0 \\ 0 \end{bmatrix} \tag{4.41}$$

The nontrivial solution to Eq. (4.41) is obtained from the condition that the main matrix determinant is equal to zero. Thus, one can obtain the frequency equation

$$\sin \lambda_2 = 0 \tag{4.42}$$

Consequently, the corresponding *i*th normal modes with simply supported boundary conditions can be obtained as

$$\begin{aligned} \varphi(x) &= H \sin \lambda_2 x, \\ \upsilon(x) &= H' \cos \lambda_2 x \end{aligned} \tag{4.43}$$

4.2.3 Galerkin's Discretization

The Galerkin truncation method is used to discretize the system and the series expansion forms for $u(x,t)$ and $\psi(x,t)$ with the simply supported boundary conditions are assumed as

$$\begin{aligned} u(x,t) &= \sum_{k=1}^{\infty} q_k(t) \varphi_k(x), \\ \psi(x,t) &= \sum_{k=1}^{\infty} \zeta_k(t) \upsilon_k(x) \end{aligned} \tag{4.44}$$

where $\varphi_k(x)$ and $\nu_k(x)$ are the trial functions, $q_k(t)$ and $\zeta_k(t)$ are the sets of generalized displacements. In this research, the trial functions $\varphi_k(x)$ and $\nu_k(x)$ are chosen as eigenfunctions of the Timoshenko beam linear subsystem with the simply supported boundary conditions as

$$\begin{aligned}\varphi_k(x) &= \sin(\beta_k x),\\ \upsilon_k(x) &= \cos(\beta_k x)\end{aligned} \tag{4.45}$$

The first n terms of Eq. (4.44) are considered in this research. Substituting Eq. (4.44) into Eq. (4.26) leads to

$$\begin{aligned}&\sum_{k=1}^{n}\left\{\left[\ddot{q}_k(t)+\mu\dot{q}_k(t)+\left[k_1+G_p(k\pi)^2+\alpha(k\pi)^2\right]q_k(t)\right]\varphi_k(x)\right\}\\ &-\alpha\left[\sum_{k=1}^{n}(k\pi)\zeta_k(t)\varphi_k(x)\right]+k_3\left[\sum_{k=1}^{n}q_k(t)\varphi_k(x)\right]^3=F_0\delta(x-vt),\\ &\sum_{k=1}^{n}\left\{\left[\ddot{\zeta}_k(t)+c_f\dot{\zeta}_k(t)+\left[k_f+(k\pi)^2+\beta\right]\zeta_k(t)\right]\upsilon_k(x)\right\}-\beta\left[\sum_{k=1}^{n}(k\pi)q_k(t)\upsilon_k(x)\right]=0\end{aligned} \tag{4.46}$$

Multiplying Eq. (4.46) by the weight functions $w_i(x)$ and integrating it over the interval of 0 and 1, the Galerkin procedure leads to the following set of 2n second-order ODES

$$\begin{aligned}&\sum_{k=1}^{n}\left\{\left[\ddot{q}_k(t)+\mu\dot{q}_k(t)+\left[k_1+G_p(k\pi)^2+\alpha(k\pi)^2\right]q_k(t)\right]\int_0^1\varphi_k(x)w_i(x)\mathrm{d}x\right\}\\ &-\sum_{k=1}^{n}\left[\alpha(k\pi)\zeta_k(t)\int_0^1\varphi_k(x)w_i(x)\mathrm{d}x\right]+k_3\int_0^1\left[\sum_{k=1}^{n}q_k(t)\varphi_k(x)\right]^3w_i(x)\mathrm{d}x=F_0w_i(vt),\\ &\sum_{k=1}^{n}\left\{\left[\ddot{\zeta}_k(t)+c_f\dot{\zeta}_k(t)+\left[k_f+(k\pi)^2+\beta\right]\zeta_k(t)\right]\int_0^1\upsilon_k(x)\nu_i(x)\mathrm{d}x\right\}\\ &-\sum_{k=1}^{n}\left[\beta(k\pi)q_k(t)\int_0^1\upsilon_k(x)\nu_i(x)\mathrm{d}x\right]=0, i=1,2,\ldots n\end{aligned} \tag{4.47}$$

Here, the weight functions $w_i(x)$ and $v_i(x)$, $i=1,2,\ldots,n$, are also chosen as eigenfunctions of the Timoshenko beam linear subsystem. That is,

$$w_i(x)=\sin(\beta_i x), v_i(x)=\cos(\beta_i x) \tag{4.48}$$

With the usual orthogonal condition, the SS boundary conditions lead to

$$\int_0^1\phi_k(x)w_i(x)\mathrm{d}x=\begin{cases}0, & k\neq i\\ 1/2, & k=i\end{cases}\qquad\int_0^1\upsilon_k(x)\nu_i(x)\mathrm{d}x=\begin{cases}0, & k\neq i\\ 1/2, & k=i\end{cases} \tag{4.49}$$

Substitution of Eq. (4.49) into Eq. (4.47) yields

$$\begin{aligned}&\ddot{q}_i(t)+\left[k_1+G_{\mathrm{p}}(i\pi)^2+\alpha(i\pi)^2\right]q_i(t)+2k_3\int_0^1\left[\sum_{k=1}^{n}q_k(t)\varphi_k(x)\right]^3 w_i(x)\mathrm{d}x\\&+\mu\dot{q}_i(t)-\alpha(i\pi)\zeta_i(t)=2F_0w_i(vt),\\&\ddot{\zeta}_i(t)+c_{\mathrm{f}}\dot{\zeta}_i(t)+\left[k_{\mathrm{f}}+(i\pi)^2+\beta\right]\zeta_i(t)-\beta(i\pi)q_i(t)=0,i=1,2,\ldots n\end{aligned}\tag{4.50}$$

The above mentioned ODES can be solved via the fourth-order Runge–Kutta method. In the numerical computation here, the initial conditions are

$$q(t)\big|_{t=0}=\dot{q}(t)\big|_{t=0}=\zeta(t)\big|_{t=0}=\dot{\zeta}(t)\big|_{t=0}=0\tag{4.51}$$

4.2.4 Numerical Results

In this part, numerical examples are given for parametric research. The physical and geometric properties of the Timoshenko beam, foundation and the moving load are listed in Table 4.2.

The vertical deflection of the beam when the load moves to the mid-point of the beam is shown in Fig. 4.8a, while the vertical deflection of beam center with time is illustrated in Fig. 4.8b. The Galerkin truncation term is set to four values, namely, a 50-term Galerkin's truncation, 75-term Galerkin's truncation, 150-term Galerkin's truncation, and 200-term Galerkin's truncation. As shown in the two plots, the transverse deflection increases for $x<80$ or $t<4$, and the biggest deflection appears at $x=80$ (with $\pm 0.2\%$ variations) or $t=4$ (with $\pm 0.15\%$ variations). After reaching the peak values, the transverse deflection decreases and tends to zero. The growth speed of the transverse deflection is almost the same as the reduced speed. The numerical results also demonstrated that there are large differences between the 50-term Galerkin truncation results with the 150-term ones and the 200-term ones. There is no doubt that the 50-term Galerkin's method is not accurate enough for the dynamic response analysis Timoshenko beams on nonlinear viscoelastic foundations subjected to a moving concentrated load, and there are discernible differences between the results of the 75-term and the 150-term Galerkin's method. Moreover, the results of the 150-term and the 200-term Galerkin's method are almost the same. Therefore, the 150-term Galerkin's method yields rather accurate results. The maximum relative differences between the maximum mid-point vertical deflections is 8.49×10^{-2} in the 50-term Galerkin's truncation and 200-term Galerkin's truncation, 4.06×10^{-2} in the 75-term Galerkin's truncation and 200-term Galerkin's truncation, and 0.74×10^{-2} in the 150-term Galerkin's truncation and 200-term Galerkin's truncation. The results are in good agreement with the research by Ding et al. [16].

Figure 4.9 shows the dependence of the convergence in terms of the vertical deflections of the beam on the system parameters. The abscissa represents the trunca-

Table 4.2 Properties of the beam, foundation, and load. (Reprinted from ref. [18], with kind permission from Springer Science+Business Media)

Item	Notation	Value	Dimensionless Value
Beam			
Young's modulus	E	6.998 GPa	–
Shear modulus	G	77 GPa	
Mass density	ρ	2373 kg/m^3	–
Height of pavement	h	0.3 m	–
Width of pavement	b	1.0 m	–
Length	L	160 m	–
Shear coefficients	k'	0.4	–
–	α	–	4.401
–	β	–	1.502×10^7
Foundation			
Linear stiffness	k_1	8×10^6 N/m^2	97.552
Nonlinear stiffness	k_3	8×10^6 N/m^4	2.497×10^6
Viscous damping	μ	0.3×10^6 Ns/m^2	39.263
Shear deformation coefficient	G_p	6.669×10^7 N	0.0318
Rocking stiffness	k_f	10^8 N	1.626×10^5
Rocking damping coefficient	c_f	1.5×10^6 N·s	2.618×10^4
Moving load			
Load	F_0	2.126×10^5 N	1.01×10^{-4}
Speed	V	20 m/s	0.01165

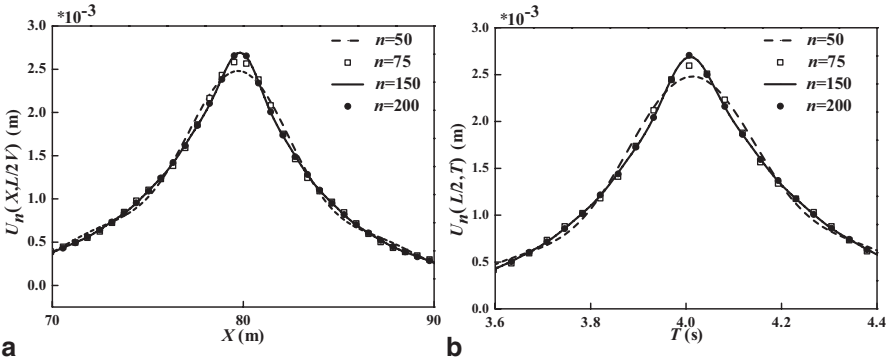

Fig. 4.8 Effects of the Galerkin's truncation terms: **a** The effects on the vertical deflection of the beam; **b** The effects on the vertical deflection of the beam's midpoint. (Reprinted from ref. [18], with kind permission from Springer Science+Business Media)

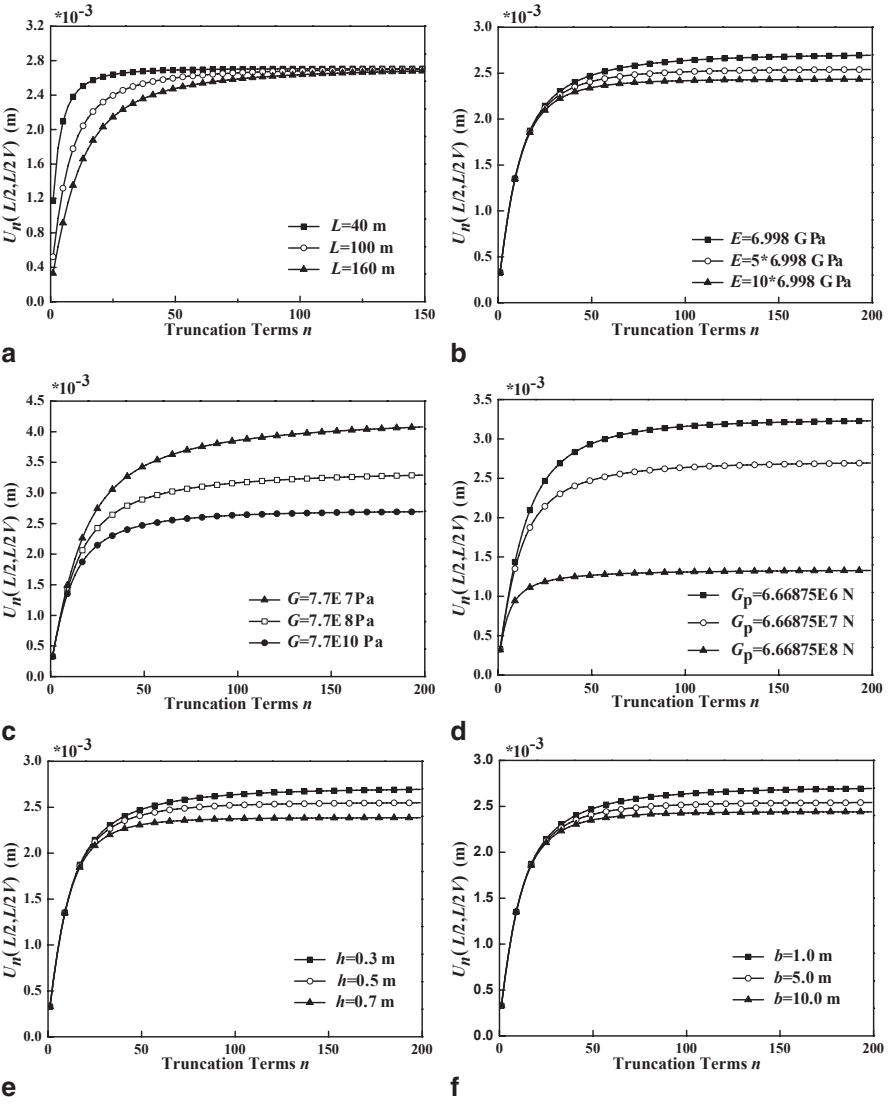

Fig. 4.9 Effects of parameters on the vertical displacements of the beam's midpoint versus the truncation terms. (Reprinted from ref. [18], with kind permission from Springer Science+Business Media)

tion terms n while the ordinate represents the vertical displacements of the beam's midpoint while $X = L/(2V)$, $T = L/(2V)$. As seen in these figures, the vertical deflections of the beam increase with the truncation terms initially, but gradually approach to a stable value. The numerical results illustrate that the convergence of the Galerkin truncation increases with the growing modulus of elasticity of the beam, the shear modulus of the beam, the shear coefficient of the foundation, the height

and the width of the beam, but decreases with the growing length of the beam. That is, the longer the length of the beam that is chosen, the more truncation terms are required to achieve convergence. From the obtained results, it is concluded that the vertical displacements of the beam decrease with the growing of these parameters except the length of the beam. For various values of L, there is little difference among the vertical deflections of the beam when $U_n(L/2, L/(2V))$ has been a stable value in Fig. 4.9a. Moreover, the numerical results also depict that there is little difference among the vertical deflections of the beam for not too large truncation terms with different values of the modulus of elasticity and the height and width of the beam. It should be noted that the effects of the above mentioned parameters have been investigated except the shear modulus of the beam and the shear coefficient of the foundation in Ref. [16]. In this section, similar conclusions are drawn from Fig. 4.9b, e and f. However, the influence of the length of the beam on the vertical deflection of a Timoshenko beam on the Pasternak foundation can be neglected, which is different from Ref. [16], probably because of a model difference.

The above discussions demonstrate that the above mentioned parameters have appreciable influences on the convergence of the Galerkin truncation. However, some parameters do not, including the linear foundation parameters, the rocking stiffness of the foundation, the damping coefficient of the foundation, and the nonlinear foundation parameters. On the other hand, these parameters have greater effects on the vertical displacements than the convergence of the Galerkin truncation. Consequently, it is difficult to demonstrate the dependence of the convergence on these parameters. In order to study the effects of these parameters on the convergence of the Galerkin truncation, δ_n is introduced and described by

$$\delta_n = \frac{U_n(L/2, L/2V) - U_{n-1}(L/2, L/2V)}{U_{n-1}(L/2, L/2V)} \times 100\% \tag{4.52}$$

The effects of other system parameters on the convergence of the Galerkin truncation are investigated in Fig. 4.10. Compared with Fig. 4.9, on the contrary, the numerical results demonstrate that δ_n decreases with the truncation terms until they are zero. From Fig. 4.10a and b, it can be seen that the convergence of the Galerkin truncation decreases with the increasing linear foundation parameters, but increases with the increasing rocking stiffness of the foundation. Furthermore, the 100-term Galerkin's method does not have a convergent numerical solution. This conclusion coincides with that in Ref. [16].

Figure 4.10c and d show a more complicated phenomenon that the convergence of the Galerkin truncation concerns not only the system parameters but also the truncation terms. As seen in Fig. 4.10c, when the truncation term is less than 37, the larger damping coefficient of the foundation performs the faster convergence. Otherwise, the smaller damping coefficient of the foundation leads to the faster convergence. A similar conclusion can be drawn from Fig. 4.10d, whereas the nonlinear foundation parameter has less influence on the convergence of the Galerkin truncation than the damping coefficient of the foundation.

The time history diagrams for the vertical dynamic deflections of the mid-span of the beam for different values of the system parameters are shown in Fig. 4.11. As seen in these figures, the maximum value of the dynamic deflection occurs almost

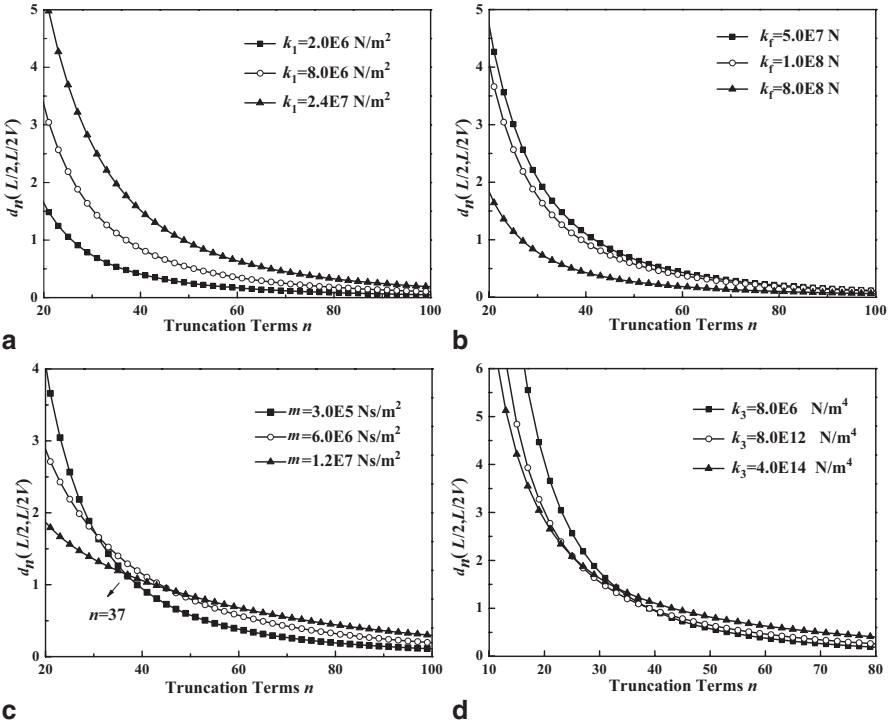

Fig. 4.10 Effects of parameters on δ_n versus truncation terms. (Reprinted from ref. [18], with kind permission from Springer Science+Business Media)

at the mid-span of the beam (with ±0.15% variations), as illustrated in Fig. 4.8b. However, it is worth to note that the peak value occurs at a farther vicinity of the mid-span (with ±0.86% variations) when the damping coefficient of the foundation is a greater one from Fig. 4.11a. Thus, the growth speed of the transverse deflection is far greater than the reduced speed. That is to say, the damping coefficient of the foundation is a reason for time delay. Moreover, as the damping coefficient of the foundation increases, the deflection of the Timoshenko beams decreases accordingly. In Ref. [19], similar results can be found. Above all, the numerical results show that the damping coefficient of the foundation has significant influence on the dynamic response of the Timoshenko beam. In other words, the damping coefficient of the foundation cannot be neglected when studying the dynamic response of finite Timoshenko beams supported by nonlinear viscoelastic Pasternak foundations.

The effects of the shear modulus of the beam and the shear deformation coefficient of the foundation on the deflections of the beams lying on viscoelastic nonlinear foundations are illustrated in Fig. 4.11b and c, respectively. From the simulation results obtained, one can see that the biggest deflections decrease with the increasing shear modulus of the beams and the increasing shear deformation coefficient of the foundations. It should be noted that a Pasternak foundation turns into a Winkler foundation when $G_p = 0$. That is to say, the maximum deflection of a Timoshenko beam on a Pasternak foundation is much smaller than that of a beam on

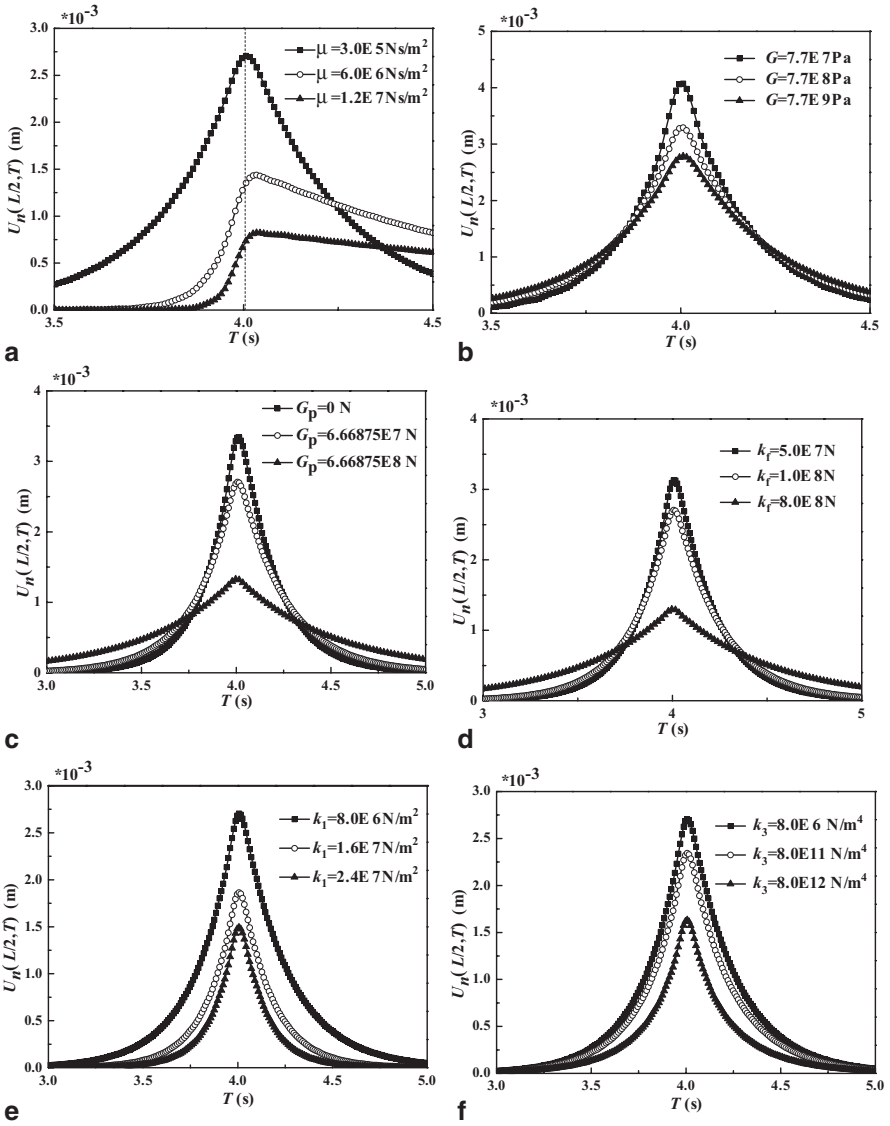

Fig. 4.11 Effects of parameters on the deflection of the beam. (Reprinted from ref. [18], with kind permission from Springer Science+Business Media)

a Winkler foundation. It is noted that this conclusion corresponds with the research in Ref. [20].

From Fig. 4.11d, one can observe that the maximum deflection decreases with the increasing rocking stiffness of the foundation. In Ref. [19], Ding et al. has a similar conclusion. Figure 4.11e and f display the effects of the linear elasticity parameter and the nonlinear elasticity parameter of the foundation on the deflection of Timoshenko beams supported by viscoelastic nonlinear foundations. The numerical

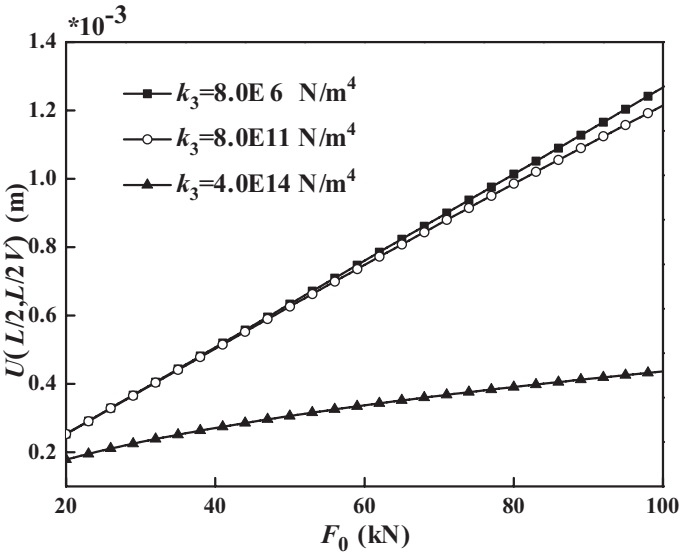

Fig. 4.12 The effects of the nonlinear elasticity parameter on the vertical displacement versus the magnitude of the moving load. (Reprinted from ref. [18], with kind permission from Springer Science+Business Media)

results indicate that the biggest deflections decrease with the increasing linear and nonlinear elasticity parameters of the foundation. The whole form of the deflection has little change with different linear elasticity parameters and nonlinear elasticity parameters of the foundation.

Figure 4.12 shows that the influence of the nonlinear elasticity parameter on the vertical displacements of the beam at mid-span while the load moves to the mid-point of the beam versus the magnitude of the moving load. The figure predicts that the difference between the results of $k_3 = 8.0 \times 10^6\,\mathrm{N/m^4}$ and $k_3 = 8.0 \times 10^{11}\,\mathrm{N/m^4}$ is very small. When compared the results of $k_3 = 8.0 \times 10^6\,\mathrm{N/m^4}$ with $k_3 = 8.0 \times 10^{14}\,\mathrm{N/m^4}$, there are big differences and the deflection decreases with the increasing nonlinear elasticity parameter. Furthermore, the deflection of the Timoshenko beams increases with the increasing magnitude of the moving load.

As far as the effects of the rocking damping coefficient on the dynamic response of finite beams are concerned, one can conclude that the rocking damping coefficient could neither affect greatly on the deflection of the beam nor make a contribution to the convergence of the Galerkin truncation from Fig. 4.13. That is, the rocking damping coefficient can be neglected when studying the dynamic response of finite Timoshenko beams supported by nonlinear viscoelastic Pasternak foundations.

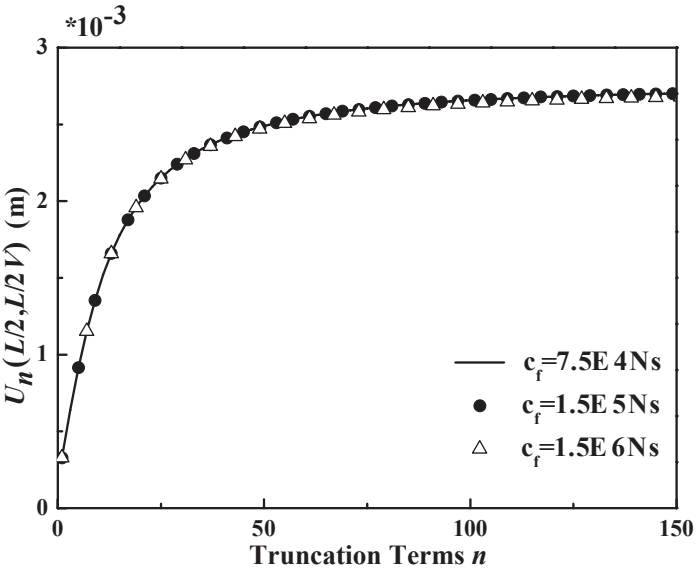

Fig. 4.13 The effects of the rocking damping coefficient on the vertical deflection versus the truncation terms. (Reprinted from ref. [18], with kind permission from Springer Science+Business Media)

4.3 Vibration of a Vehicle–Pavement Coupled System Based on a Finite Timoshenko Beam on a Nonlinear Foundation [21]

4.3.1 The Mathematical Model

The schematic of a finite elastic beam subjected to a moving spring–mass–damper system on a nonlinear foundation is shown in Fig. 4.14. The beam is modeled based on Timoshenko beam theory. $U(X, T)$ and $\psi(X, T)$ are the vertical displacement function and the slope function due to bending of the beam, respectively. T is the time. X and Z are, respectively, the spatial coordinate along the axis of the beam and the vertical spatial coordinate. Shearing strain γ is defined as $\gamma = U_{,X} - \psi$, where the comma preceding X denotes the partial differentiation with respect to X. The foundation model is characterized by linear elastic modulus k_1, nonlinear elastic modulus k_3, Pasternak foundation modulus (shear deformation coefficient) G_p, damping coefficient μ, rocking stiffness k_f, and rocking damping coefficients c_f. V represents the speed of the moving oscillator. k and c are, respectively, the elastic stiffness and the damping coefficients of the moving oscillator. m_1 and m_2 are the masses in the moving oscillator. Z_1 and Z_2 are the vertical displacement functions of the two masses of the oscillator.

Consider the pavement as a homogeneous beam with constant cross-section A, moment of inertial I, length L, densityρ, shear modulus G, effective area $k'A$, and

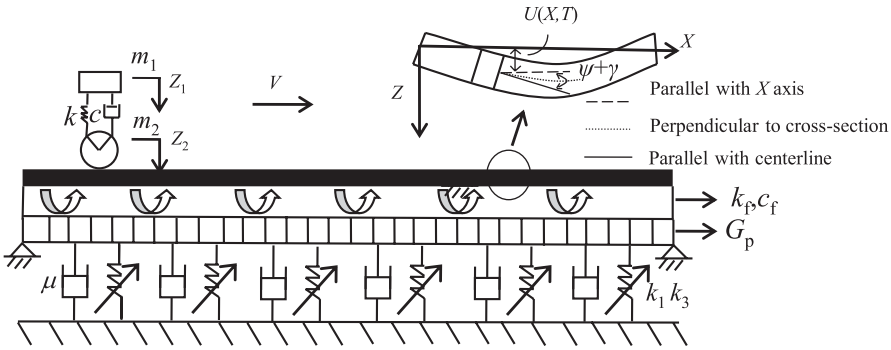

Fig. 4.14 Schematic representation of a Timoshenko beam subjected to a moving oscillator on a nonlinear Pasternak foundation. (Reprinted from ref. [21], Copyright 2014, with permission from Elsevier)

modulus of elasticity E. The equations of motion for the Timoshenko beam can be obtained by the d'Alembert's principle and the Timoshenko beam theory as

$$\begin{aligned}&\rho AU_{,TT}+k'AG\left(\psi_{,X}-U_{,XX}\right)+k_1U+k_3U^3+\mu U_{,T}-G_pU_{,XX}=F_0\delta\left(X-VT\right),\\&\rho I\psi_{,TT}-EI\psi_{,XX}+k'AG\left(\psi-U_{,X}\right)+k_f\psi+c_f\psi_{,T}=0\end{aligned}\tag{4.53}$$

where F_0 represents the force induced by the moving spring–mass–damper oscillator. The comma preceding T denotes the partial differentiation with respect to T. Furthermore, the equations of motion for the moving oscillator can be obtained by Newton's Second Law as

$$\begin{aligned}&m_1\frac{\mathrm{d}^2Z_1}{\mathrm{d}T^2}+k\left(Z_1-Z_2\right)+c\left(\frac{\mathrm{d}Z_1}{\mathrm{d}T}-\frac{\mathrm{d}Z_2}{\mathrm{d}T}\right)=0,\\&m_2\frac{\mathrm{d}^2Z_2}{\mathrm{d}T^2}-k\left(Z_1-Z_2\right)-c\left(\frac{\mathrm{d}Z_1}{\mathrm{d}T}-\frac{\mathrm{d}Z_2}{\mathrm{d}T}\right)=-F_0+m_1g+m_2g\end{aligned}\tag{4.54}$$

In this research, all work is based on the assumption that the moving oscillator stays on the ground. The displacement of the moving oscillator is expressed as the sum of the vertical displacement of the beam and beam's surface roughness as

$$Z_2(T)=U(X,T)|_{X=VT}+\mathrm{Z_p}(X)|_{X=VT}\tag{4.55}$$

where $\mathrm{Z_p}(X)$ represents the road surface roughness, and is defined as

$$\mathrm{Z_p}(X)=a\sin\left(\frac{2\pi X}{L_0}\right)\tag{4.56}$$

in which a is the amplitude of the road surface roughness, and L_0 is the wavelength of harmonic road roughness. Substituting Eq. (4.55) into Eq. (4.54) leads to

$$m_1\frac{\mathrm{d}^2 Z_1}{\mathrm{d}T^2}=-k(Z_1-Z_2)-c\frac{\mathrm{d}Z_1}{\mathrm{d}T}+c\left[U_{,T}+VU_{,X}+V\frac{\mathrm{d}Z_{\mathrm{p}}(X)}{\mathrm{d}X}\right]_{X=VT} \tag{4.57}$$

and

$$\begin{aligned}F_0=&-m_2\left[U_{,TT}+2VU_{,XT}+V^2U_{,XX}+V^2\frac{\mathrm{d}^2 Z_{\mathrm{p}}(X)}{\mathrm{d}X^2}\right]_{X=VT}+k(Z_1-Z_2)\\&+c\frac{\mathrm{d}Z_1}{\mathrm{d}T}-c\left[U_{,T}+VU_{,X}+V\frac{\mathrm{d}Z_{\mathrm{p}}(X)}{\mathrm{d}X}\right]_{X=VT}+m_1g+m_2g\end{aligned} \tag{4.58}$$

Substitution of Eqs. (4.57) and (4.58) into Eq. (4.53) leads to the following governing differential equations of coupled motion

$$\begin{aligned}&\rho AU_{,TT}+k'AG(\psi_{,X}-U_{,XX})+k_1U+k_3U^3+\mu U_{,T}-G_{\mathrm{p}}U_{,XX}=\\&\left\{-m_2\left[Y_{,TT}+2VY_{,XT}+V^2Y_{,XX}+V^2\frac{\mathrm{d}^2 Z_{\mathrm{p}}(X)}{\mathrm{d}T^2}\right]_{X=VT}+(m_2+m_1)g-m_1\frac{\mathrm{d}^2 Z_1}{\mathrm{d}T^2}\right\}\delta(X-VT),\\&\rho I\psi_{,TT}-EI\psi_{,XX}+k'AG(\psi-U_{,X})+k_{\mathrm{f}}\psi+c_{\mathrm{f}}\psi_{,T}=0,\\&m_1\frac{\mathrm{d}^2 Z_1}{\mathrm{d}T^2}=-k\{Z_1-[U+Z_{\mathrm{p}}(X)]_{X=VT}\}-c\left\{\frac{\mathrm{d}Z_1}{\mathrm{d}T}-\left[U_{,T}+VU_{,X}+V\frac{\mathrm{d}Z_{\mathrm{p}}(X)}{\mathrm{d}X}\right]_{X=VT}\right\}\end{aligned} \tag{4.59}$$

Here, the beam is assumed to be simply supported at both ends. Therefore, the boundary conditions are given as follows

$$U(X,T)\big|_{X=0}=U(X,T)\big|_{X=L}=0,EI\psi_{,X}(X,T)\big|_{X=0}=EI\psi_{,X}(X,T)\big|_{X=L}=0 \tag{4.60}$$

In order to avoid round-off due to manipulations with large or small numbers in numerical calculations, the following dimensionless variables and parameters are introduced

$$\begin{aligned}&u=\frac{U}{L},t=\frac{T}{L}\sqrt{\frac{E}{\rho}},x=\frac{X}{L},\psi=\psi,v=V\sqrt{\frac{\rho}{E}},\alpha=\frac{k'G}{E},\beta=k'AG\frac{L^2}{EI},\\&\kappa=\frac{(m_2+m_1)g}{EA},z_{\mathrm{p}}=\frac{a}{L}\sin\left(\frac{2\pi xL}{L_0}\right),z_1=\frac{Z_1}{L},k\leftrightarrow\frac{\rho L^2}{m_1E}k,k_1\leftrightarrow\frac{k_1L^2}{EA},\\&k_3\leftrightarrow\frac{k_3L^4}{EA},\mu\leftrightarrow\frac{\mu}{A}\sqrt{\frac{L^2}{\rho E}},G_{\mathrm{p}}\leftrightarrow G_{\mathrm{p}}\frac{1}{EA},k_{\mathrm{f}}\leftrightarrow k_{\mathrm{f}}\frac{L^2}{EI},c_{\mathrm{f}}\leftrightarrow\frac{\mathrm{c}_{\mathrm{f}}}{\mathrm{I}}\sqrt{\frac{L^2}{\rho E}},\\&m_2\leftrightarrow\frac{m_2}{\rho AL},m_1\leftrightarrow\frac{m_1}{\rho AL},c\leftrightarrow\frac{cL}{m_1}\sqrt{\frac{\rho}{E}}\end{aligned} \tag{4.61}$$

Equations (4.59) and (4.60) can be expressed into the dimensionless normalized forms

$$\begin{aligned}
&u_{,tt}+\alpha\left(\psi_{,x}-u_{,xx}\right)+k_1u+k_3u^3+\mu u_{,t}-G_{\mathrm{p}}u_{,xx}\\
&\quad=\left[\kappa-m_1\frac{\mathrm{d}^2z_1}{\mathrm{d}t^2}-m_2\left(y_{,tt}+2vy_{,xt}+v^2y_{,xx}+v^2\frac{\mathrm{d}^2z_{\mathrm{p}}}{\mathrm{d}x^2}\right)_{x=vt}\right]\delta\left(x-vt\right),\\
&\psi_{,tt}-\psi_{,xx}+\beta\left(\psi-u_{,x}\right)+k_{\mathrm{f}}\psi+c_{\mathrm{f}}\psi_{,t}=0,\\
&\frac{\mathrm{d}^2z_1}{\mathrm{d}t^2}+k\left[z_1-\left(u+z_{\mathrm{p}}\right)_{x=vt}\right]+c\left[\frac{\mathrm{d}z_1}{\mathrm{d}t}-\left(u_{,t}+vu_{,x}+v\frac{\mathrm{d}z_{\mathrm{p}}}{\mathrm{d}x}\right)_{x=vt}\right]=0
\end{aligned}\tag{4.62}$$

and

$$u\left(x,t\right)\big|_{x=0}=u\left(x,t\right)\big|_{x=1}=0,\psi_{,x}\left(x,t\right)\big|_{x=0}=\psi_{,x}\left(x,t\right)\big|_{x=1}=0\tag{4.63}$$

4.3.2 The Schemes of Solution

The Galerkin truncation method is used to discretize the governing equations and the series expansion form for $u(x, t)$ and $\psi(x, t)$ which are simply supported at both ends, respectively, are assumed as

$$\begin{aligned}
u\left(x,t\right)&=\sum_{k=1}^{\infty}q_k\left(t\right)\varphi_k\left(x\right),\\
\psi\left(x,t\right)&=\sum_{k=1}^{\infty}\zeta_k\left(t\right)\upsilon_k\left(x\right)
\end{aligned}\tag{4.64}$$

where $q_k(t)$ and $\zeta_k(t)$, respectively, are sets of generalized vertical displacements and slope displacements due to the bending of the beam, $\varphi_k(x)$ and $\nu_k(x)$ are the trial functions of $u(x, t)$ and $\psi(x, t)$, respectively. Moreover, each of the trial functions should satisfy the boundary conditions (4.63). The first n terms of Eq. (4.64) are considered in the following calculations.

In this research, the trial functions $\varphi_k(x)$ and $\nu_k(x)$ are chosen as eigenfunctions of the Timoshenko beam linear subsystem with the simply supported boundary conditions as

$$\begin{aligned}
\varphi_k\left(x\right)&=\sin\left(\beta_kx\right),\\
\upsilon_k\left(x\right)&=\cos\left(\beta_kx\right)
\end{aligned}\tag{4.65}$$

where $\beta_k=k\pi$. Substituting Eqs. (4.64) and (4.65) into Eq. (4.62) leads to

$$\begin{aligned}
&\sum_{k=1}^{n}\left\{\left[\ddot{q}_k(t)+\mu\dot{q}_k(t)+\left(k_1+G_p\beta_k{}^2+\alpha\beta_k{}^2\right)q_k(t)\right]\sin(\beta_k x)\right\}-\alpha\sum_{k=1}^{n}\beta_k\zeta_k(t)\sin(\beta_k x)\\
&\quad+k_3\left[\sum_{k=1}^{n}q_k(t)\sin(\beta_k x)\right]^3+\left\{m_1\ddot{z}_1(t)-\kappa+m_2\left[\sum_{k=1}^{n}\ddot{q}_k(t)\sin(\beta_k vt)+2v\sum_{k=1}^{n}\beta_k\dot{q}_k(t)\cos(\beta_k vt)\right.\right.\\
&\quad\left.\left.-v^2\sum_{k=1}^{n}\beta_k{}^2q_k(t)\sin(\beta_k vt)-\frac{4\pi^2v^2aL}{L_0{}^2}\sin\left(\frac{2\pi vtL}{L_0}\right)\right]\right\}\delta(x-vt)=0,\\
&\sum_{k=1}^{n}\left\{\left[\ddot{\zeta}_k(t)+c_f\dot{\zeta}_k(t)+\left(k_f+\beta_k{}^2+\beta\right)\zeta_k(t)\right]\cos(\beta_k x)\right\}-\beta\sum_{k=1}^{n}\beta_k q_k(t)\cos(\beta_k x)=0,\\
&\ddot{z}_1(t)+kz_1(t)-k\sum_{k=1}^{n}q_k(t)\sin(\beta_k vt)-k\frac{a}{L}z_p(vt)+c\dot{z}_1(t)-c\sum_{k=1}^{n}\dot{q}_k(t)\sin(\beta_k vt)\\
&\quad-cv\sum_{k=1}^{n}\beta_k q_k(t)\cos(\beta_k vt)-\frac{2\pi cva}{L_0}\cos\left(\frac{2\pi vtL}{L_0}\right)=0
\end{aligned}\tag{4.66}$$

Here, the weight functions $w_i(x)$ and $v_i(x)$, $i=1,2,\ldots,n$, are also chosen as eigenfunctions of the Timoshenko beam linear subsystem, i.e.,

$$w_i(x)=\sin(\beta_i x),v_i(x)=\cos(\beta_i x)\tag{4.67}$$

Multiplying the first two equations of Eq. (4.66) by the weight functions $w_i(x)$ and $v_i(x)$, respectively, then integrating the resulting equation over the interval of 0 and 1, the Galerkin procedure leads to the following set of $2n+1$ s-order ODES

$$\begin{aligned}
&\ddot{q}_i(t)+\mu\dot{q}_i(t)+\left(k_1+G_p\beta_i{}^2+\alpha\beta_i{}^2\right)q_i(t)-\alpha\beta_i\zeta_i(t)+2k_3\int_0^1\left[\sum_{k=1}^{n}q_k(t)\sin(\beta_k x)\right]^3\sin(\beta_i x)\mathrm{d}x\\
&\quad-2\kappa\sin(\beta_i vt)+2m_1\ddot{z}_1(t)\sin(\beta_i vt)+2m_2\left[\sum_{k=1}^{n}\ddot{q}_k(t)\sin(\beta_k vt)\right]\sin(\beta_i vt)\\
&\quad+4m_2v\left[\sum_{k=1}^{n}\beta_k\dot{q}_k(t)\cos(\beta_k vt)\right]\sin(\beta_i vt)-2m_2v^2\left[\sum_{k=1}^{n}\beta_k{}^2q_k(t)\sin(\beta_k vt)\right]\sin(\beta_i vt)\\
&\quad-\frac{8\pi^2v^2m_2aL}{L_0{}^2}\sin\left(\frac{2\pi vtL}{L_0}\right)\sin(\beta_i vt)=0,\\
&\ddot{\zeta}_i(t)+c_f\dot{\zeta}_i(t)+\left(k_f+\beta_i{}^2+\beta\right)\zeta_i(t)-\beta\beta_i q_i(t)=0,i=1,2,\ldots n,\\
&\ddot{z}_1(t)+kz_1(t)-k\sum_{k=1}^{n}q_k(t)\sin(\beta_k vt)-k\frac{a}{L}\sin\left(\frac{2\pi vtL}{L_0}\right)+c\dot{z}_1(t)-c\sum_{k=1}^{n}\dot{q}_k(t)\sin(\beta_k vt)\\
&\quad-cv\sum_{k=1}^{n}\beta_k q_k(t)\cos(\beta_k vt)-\frac{2\pi cva}{L_0}\cos\left(\frac{2\pi vtL}{L_0}\right)=0
\end{aligned}\tag{4.68}$$

In the following simulations, the initial conditions are all set as

$$\begin{aligned}
&q(t)\big|_{t=0}=0,q_{,t}(t)\big|_{t=0}=0,\\
&\zeta(t)\big|_{t=0}=0,\zeta_{,t}(t)\big|_{t=0}=0,\\
&z_1(t)\big|_{t=0}=0,z_{1,t}(t)\big|_{t=0}=0
\end{aligned}\tag{4.69}$$

For a set of given physical and geometric parameters of the Timoshenko beam, the foundation and the moving vehicle, $q_k(t)$, $\zeta_k(t)$, and $z_1(t)$ can be numerically solved via the fourth-order Runge–Kutta method from Eq. (4.68) by discretizing the temporal variables based on the initial conditions of Eq. (4.69). After substituting the numerical solutions of $q_k(t)$ and $\zeta_k(t)$ into Eq. (4.64), one can solve the vertical displacement function $u(x, t)$ and the slope function $\psi(x, t)$.

4.3.3 Numerical Case Studies

In the following numerical examples, the physical and geometric properties of the vehicle–pavement coupled system are listed in Table 4.3.

Based on the parameter values, the values of the dimensionless parameters α, β, and κ, are determined by Eq. (4.61) as $\alpha = 4.4013, \beta = 1.502 \times 10^7$, and $k = 1.02172 \times 10^{-4}$.

Ride comfort is one of the most significant dynamic performance characteristics of modern vehicles. Here, the vertical dynamic acceleration of the vehicle body, m_1, is introduced for describing the ride comfort. Therefore, the acceleration A_1 is defined as

Table 4.3 Properties of the Timoshenko beam, foundation and load. (Reprinted from ref. [21], Copyright 2014, with permission from Elsevier)

	Item	Notation	Value	Dimensionless value
Vehicle	Vehicle body mass	m_1	21260 kg	0.18665
	Tire mass	m_2	190 kg	0.00167
	Suspension stiffness	k	2.06×10^6 N/m	0.84114
	Suspension damping	c	3.0×10^4 N s/m	0.13151
	Speed	V	15 m/s	0.00874
Foundation	Linear stiffness	k_1	8×10^6 N/m^2	97.552
	Nonlinear stiffness	k_3	8×10^6 N/m^4	2.497×10^6
	Viscous damping	μ	0.3×10^6 Ns/m^2	39.263
	Shear parameter	G_p	6.66875×10^7 N	0.0318
	Rocking stiffness	k_f	10^6 N	1.6259×10^3
	Rocking damping coefficient	c_f	1.5×10^6 N·s	2.618×10^4
Beam	Young's modulus	E	6.998 GPa	–
	Shear modulus	G	3.2 GPa	–
	Mass density	ρ	2373 kg/m^3	–
	Cross–section of the pavement	A	0.3 m^2	–
	Moment of inertial of the pavement	I	0.00225 m^4	–
	Length	L	160 m	–
	Wavelength of road roughness	L_0	10 m	
	Amplitude of road roughness	a	0.002 m	
	Shear coefficients	k'	0.4	–

$$A_1 = \frac{\mathrm{d}^2 Z_1}{\mathrm{d}T^2} \tag{4.70}$$

Convergence Studies

The modal truncation method has been widely used to investigate the dynamic response of elastic materials on a nonlinear foundation. Theoretically, an exact solution is obtained by considering an infinite number of modes. Ding et al. studied the convergence of Galerkin's method for the Euler–Bernoulli beam [16] and the Timoshenko beam [18] on a nonlinear foundation subjected to a moving force. The authors found that the Galerkin truncation needs super high-order modes. Moreover, Bhattiprolu, Bajaj, and Davies studied the effect of the number of modes due to the nonlinear and viscoelastic behaviors of soils [22]. They found that Galerkin's method needs 20 modes even for the beam on a nonlinear foam foundation. At the beginning of the numerical investigation, the convergence of the modal truncation is studied for determining the validity of the present study.

Figure 4.15 shows the comparison of the dynamic responses of the vehicle–pavement coupled system with different Galerkin truncation terms. The time history of the vertical deflection of the midpoint of the Timoshenko beam, meaning $X = L/2$, is shown in Fig. 4.15a. The vertical deflection $U(X, L/2V)$ of the Timoshenko beam is shown in Fig. 4.15b. As shown in Fig. 4.15a and b, there are significant differences between the results from the 25-term modal truncation with the results from the 100-term truncation and the 200-term truncation. Furthermore, there are some differences that can be discerned from the numerical results of the 50-term modal truncation with the results of the 100-term. Therefore, the dynamic response of the Timoshenko beam on a six-parameter foundation subjected to a moving oscillator needs more than 50 terms of the modal truncation. The comparison also shows that the vertical deflections from the 100-term modal truncation are very close to the results from the 200-term truncation. These conclusions are in good agreement with the study by Yang et al. based on the same pavement and subgrade model subjected to a moving force [18].

Figure 4.15c and d, respectively, display the vertical displacement and the acceleration of the vehicle body with the different terms of the modal truncation. Figure 4.15c shows that there are discernible differences between the time history and the vertical displacement of the vehicle body of 25-term and 200-term modal truncations. Moreover, Fig. 4.14d illustrates that there are almost no differences in the accelerations of the vehicle body between the 25-term and 200-term modal truncation. Therefore, the simulations for the displacement of the vehicle body do not need such a large number of modes as like the calculations for the displacement of the pavement do.

From Fig. 4.15a–d, one can find that the 100-term Galerkin truncation for the dynamic response of the vehicle–pavement coupled system based on a Timoshenko beam on a six-parameter foundation yields rather accurate results. In the following numerical examples, the first 100 modes are considered for the Galerkin truncation. Therefore, $n = 100$.

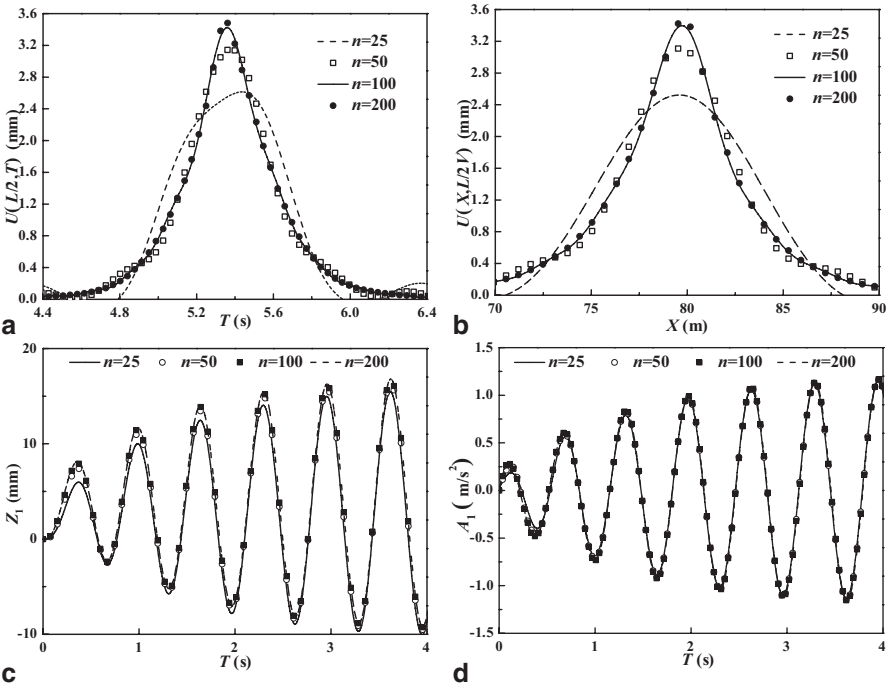

Fig. 4.15 Convergence of the Galerkin's truncation method. (Reprinted from ref. [21], Copyright 2014, with permission from Elsevier)

The Timoshenko beam theory takes into account shear deformation and rotational inertia effects. If the shear deformation and the rotational inertia effects are neglected, the Timoshenko beam theory deduces to the Euler–Bernoulli beam theory. The Euler–Bernoulli beam theory is known as an engineer's beam theory or classical beam theory. The similar Galerkin procedure is applicable in the case of Euler–Bernoulli beams on the same nonlinear foundation. In this case, the equations of motion can be derived as

$$\rho A U_{,TT} + EIU_{,XXXX} + k_1 U + k_3 U^3 + \mu U_{,T} - G_p U_{,XX} =$$
$$\left\{ -m_2 \left[U_{,TT} + 2VU_{,XT} + V^2 U_{,XX} + V^2 \frac{\mathrm{d}^2 Z_p(X)}{\mathrm{d}X^2} \right]_{X=VT} \right.$$
$$\left. + (m_2 + m_1) g - m_1 \frac{\mathrm{d}^2 Z_1}{\mathrm{d}T^2} \right\} \delta(X - VT),$$
$$m_1 \frac{\mathrm{d}^2 Z_1}{\mathrm{d}T^2} = -k\{Z_1 - [U + Z_P(X)]_{X=VT}\} - c\left\{ \frac{\mathrm{d}Z_1}{\mathrm{d}T} - \left[U_{,T} + VU_{,X} + V\frac{\mathrm{d}Z_p(X)}{\mathrm{d}X} \right]_{X=VT} \right\} \tag{4.71}$$

Using the similar Galerkin procedure, the following set of $n+1$ dimensionless second-order ODES leads to

$$\begin{aligned}
&\ddot{q}_i(t)+\mu\dot{q}_i(t)+2k_3\int_0^1\left[\sum_{k=1}^{n}q_k(t)\sin(\beta_k x)\right]^3\sin(\beta_i x)\mathrm{d}x+\sin(\beta_i vt)\\
&\left\{2m_2\left[\sum_{k=1}^{n}\ddot{q}_k(t)\sin(\beta_k vt)\right]+2m_1\ddot{z}_1(t)-2\kappa+4m_2v\left[\sum_{k=1}^{n}\beta_k\dot{q}_k(t)\cos(\beta_k vt)\right]\right.\\
&\left.-2m_2v^2\left[\sum_{k=1}^{n}\beta_k{}^2q_k(t)\sin(\beta_k vt)\right]-8\mathrm{m}_2v^2\frac{\pi^2aL}{L_0{}^2}\sin\left(\frac{2\pi vtL}{L_0}\right)\right\}\\
&+\beta_i{}^2G_{\mathrm{p}}q_i(t)+\beta_i{}^4k_{\mathrm{b}}{}^2q_i(t)+k_1q_i(t)=0,\ \ i=1,2,...n,\\
&\ddot{z}_1(t)=-kz_1(t)+k\sum_{k=1}^{n}q_k(t)\sin(\beta_k vt)+k\frac{a}{L}\sin\left(\frac{2\pi vtL}{L_0}\right)+c\sum_{k=1}^{n}\dot{q}_k(t)\sin(\beta_k vt)\\
&+\frac{2\pi cva}{L_0}\cos\left(\frac{2\pi vtL}{L_0}\right)-c\dot{z}_1(t)+cv\sum_{k=1}^{n}\beta_k q_k(t)\cos(\beta_k vt)
\end{aligned}\tag{4.72}$$

where dimensionless parameter k_{b} is defined as

$$k_{\mathrm{b}}=\frac{1}{L}\sqrt{\frac{I}{A}}\tag{4.73}$$

Based on the parameter values in Table 4.3, k_{b} is determined by Eq. (4.73) as $k_b=5.41\times10^{-4}$. Then, $q_k(t)$ and $z_1(t)$ in Eq. (4.72) are numerically solved via the fourth-order Runge–Kutta method.

In Fig. 4.16a, the effects of two different beam theories on the vertical displacements of the pavement $U(L/2,L/2V)$ versus the truncation terms are shown. Without considering the rocking stiffness and the rocking damping coefficients, the numerical results in Fig. 4.16a illustrate that the convergence of the Galerkin

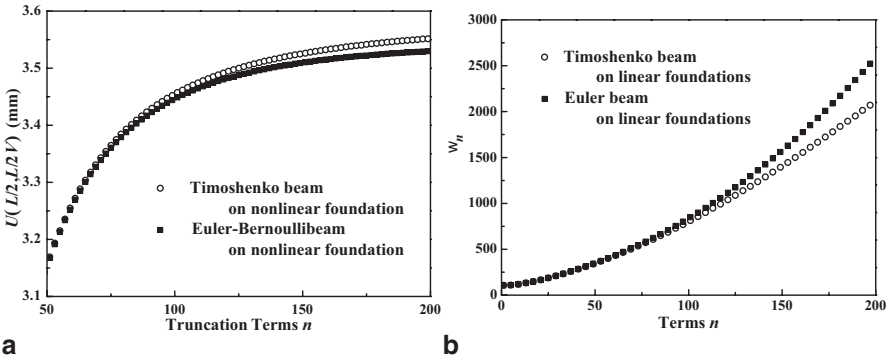

Fig. 4.16 Comparison between the different beam theories of the pavement. (Reprinted from ref. [21], Copyright 2014, with permission from Elsevier)

truncation for the Timoshenko beam on the six-parameter foundation is slightly slower than the Euler–Bernoulli beam on the same foundation. Moreover, Fig. 4.16a shows that the vertical displacements of the Timoshenko beam are slightly larger than those of the Euler–Bernoulli beam. One thing needs to be known, Palmeri and Cicirello also found that the Timoshenko beam theory predicts larger deflections than the Euler–Bernoulli beam theory based on cracked beams under static loads [23]. In Ref. [16], the authors have found that the convergence of the modal truncation is predicted by the natural frequency of the linear subsystem. In order to explore the reason behind the different convergence for the two beam theories, the natural frequencies of the linear subsystem of the two beam models are compared. The natural frequencies of the Euler–Bernoulli beam on a linear elastic Pasternak foundation which is simply supported and without any loads, $\omega \mathrm{E}_k$, are derived as follows

$$\omega_{\mathrm{E}k}^2 = k_{\mathrm{b}}^2 (k\pi)^4 + k_1 + G_{\mathrm{P}} (k\pi)^2 \tag{4.74}$$

where $k = 1,2,\ldots$. The natural frequencies of the Timoshenko beam on the same foundation and with the same boundary conditions, $\omega \mathrm{T}_k$, are calculated from the following equation

$$\sqrt{\sqrt{\left(\frac{\omega_{\mathrm{T}k}^2 - k_1 + (\alpha + G_{\mathrm{p}})(\omega_{\mathrm{T}k}^2 - \beta) + \alpha\beta}{\alpha + G_{\mathrm{p}}}\right)^2 - 4\frac{(\omega_{\mathrm{T}k}^2 - k_1)(\omega_{\mathrm{T}k}^2 - \beta)}{\alpha + G_{\mathrm{p}}}} + \frac{\omega_{\mathrm{T}k}^2 - k_1 + (\alpha + G_{\mathrm{p}})(\omega_{\mathrm{T}k}^2 - \beta) + \alpha\beta}{\alpha + G_{\mathrm{p}}}} = \sqrt{2}k\pi \tag{4.75}$$

The Fig. 4.16b shows that the natural frequencies of the Timoshenko beam on a linear foundation increase slower than the frequencies of the Euler–Bernoulli beam on the same foundation. The comparison between Fig. 4.16a and b shows that the changing tendencies of the natural frequencies not only predict the convergence of the modal truncation, but also predict the differences between the convergences of the different beam theories.

Figure 4.17 shows the effects of the length of the road on the dynamic response of the pavement. Figure 4.17a and b, respectively, depict the effects of the length of the road for the Euler–Bernoulli beam and the Timoshenko beam on a nonlinear foundation. As indicated by Fig. 4.17, the vertical displacement of the pavement does not converge with an increasing length of the road. Furthermore, the no convergence phenomenon appears in the dynamic response based on the Euler–Bernoulli beam and the Timoshenko beam on a nonlinear foundation. The amplitude of the fluctuation of the vertical displacement is about 1/10 of the maximum vertical deflection of the pavement. It should be noted that Thambiratnam and Zhuge found that the finite length of beams can accurately approximate the response of the ideal beam of infinite length based on the dynamic analysis of beams on an elastic foundation subjected to moving point loads [24]. Moreover, based on a moving concentrated load, Ding et al. also found the dynamic responses have good convergence of the length of the pavement [16]. Therefore, the coupling between the oscillator and

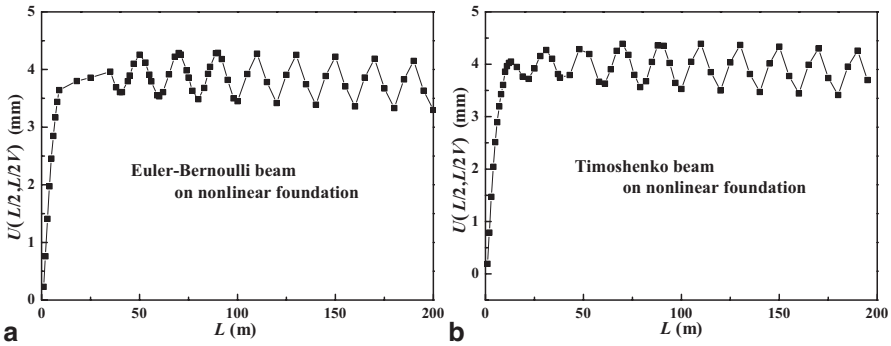

Fig. 4.17 The effects of the length of the road on the vertical displacement of the pavement midpoint. (Reprinted from ref. [21], Copyright 2014, with permission from Elsevier)

the pavement causes the fluctuation of the vertical displacement of the pavement with the increasing length of the road. On the other hand, Fig. 4.17 illustrates that the maximum and the minimum of the fluctuation of the vertical displacement are both convergent with an increasing pavement length. Therefore, the finite length of the pavement can be used to study the vibration of the vehicle–pavement coupled system. In the following calculations, the length of the road, $L = 160$ m.

The Coupling Effect

The effect of coupling between the pavement and the vehicle is examined in this section. Based on Eq. (4.56) and Table 4.3, the excitation frequency from the roughness of the road surface is derived as

$$\omega_P = \frac{2\pi V}{L_0} = 9.425 \tag{4.76}$$

If the suspension damping is neglected, based on Table 4.3, the natural frequency of the moving spring–mass oscillator is derived as

$$\omega_o = \sqrt{\frac{k}{m_1}} = 9.844 \tag{4.77}$$

Therefore, based on the parameter values in Table 4.3, the vehicle body is near to resonance.

The time history of the vertical displacement of the pavement $U(L/2, T)$ is described in Fig. 4.18a. Meanwhile, the time history of the vehicle body is shown in Fig. 4.18b. The speed of the moving vehicle is set to three values, namely, $V = 10$ m/s, $V = 15.667$ m/s, and $V = 20$ m/s. Based on Eq. (4.76) and Table 4.3, the excitation frequencies of the pavement, respectively, are calculated as $\omega_P = 6.283$ rad/s,

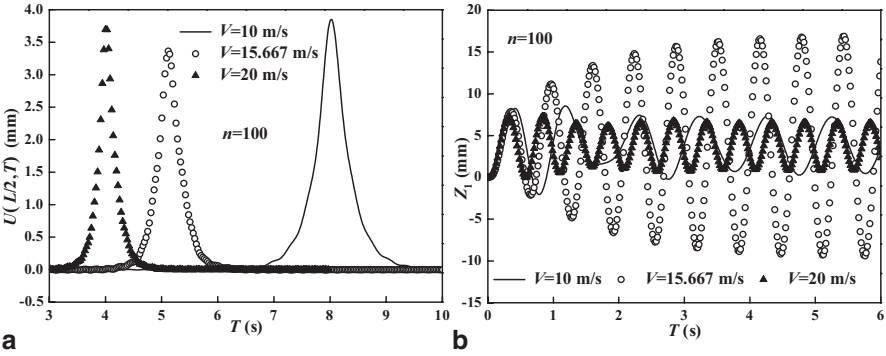

Fig. 4.18 The effects of the speed of the vehicle. (Reprinted from ref. [21], Copyright 2014, with permission from Elsevier)

ω_p=9.844 rad/s, and ω_p=12.566 rad/s. Figure 4.18b shows that the amplitude of the vibration of the vehicle is very large when the vehicle is near to resonance. Based on Eq. (4.76), the vibration of the vehicle will be faster for the greater moving speed. This conclusion is also found from Fig. 4.18b. Figure 4.18a reveals that the amplitude of the dynamic response of the pavement becomes smaller when the vehicle is close to resonance. Furthermore, the response curves of the midpoint of the beam become narrower when the moving speed of the vehicle increases. Therefore, the resonance of the vehicle obviously influences the dynamic response of the pavement.

Figure 4.19a exhibits the biggest displacement of the vehicle body versus the speed of the vehicle. The numerical results clearly show the resonance area of the vehicle body. Moreover, there is only a little change for the biggest displacement of the vehicle body with the different moving speeds of the vehicle while speeding away from the resonance area. Figure 4.19b and c, respectively, show the biggest vertical displacement of the midpoint of the pavement and the biggest acceleration of the vehicle body versus the moving speed of the vehicle. The comparison between Fig. 4.19b and c clearly reveals that the changing tendencies of the vertical deflections of the pavement's midpoint and the acceleration of the vehicle body versus the speed are completely opposite. On the other hand, the changing processes of Fig. 4.19a and b are fully synchronized. Therefore, the dynamic response of the pavement and the vibration of the vehicle are coupled.

Figure 4.20a and b show the time history of the midpoint of the pavement and the vehicle body with different suspension stiffness. Based on Eq. (4.76) and Table 4.3, the natural frequencies of the vehicle are calculated as ω_o=0.9844 rad/s for $k = 2.06 \times 10^4\,\mathrm{N/m}$ and ω_o=31.49 rad/s for $k = 2.06 \times 10^7\,\mathrm{N/m}$. Therefore, the vehicle is far away from resonance when $k = 2.06 \times 10^4\,\mathrm{N/m}$ and $k = 2.06 \times 10^7\,\mathrm{N/m}$. This is the reason why the vibration of the vehicle body is very weak with $k = 2.06 \times 10^4\,\mathrm{N/m}$ and $k = 2.06 \times 10^7\,\mathrm{N/m}$. Figure 4.21 illustrates the influence of the suspension damping on the dynamic response of the vehicle–pavement coupled system. Figure 4.21b shows that the vibration of the vehicle becomes

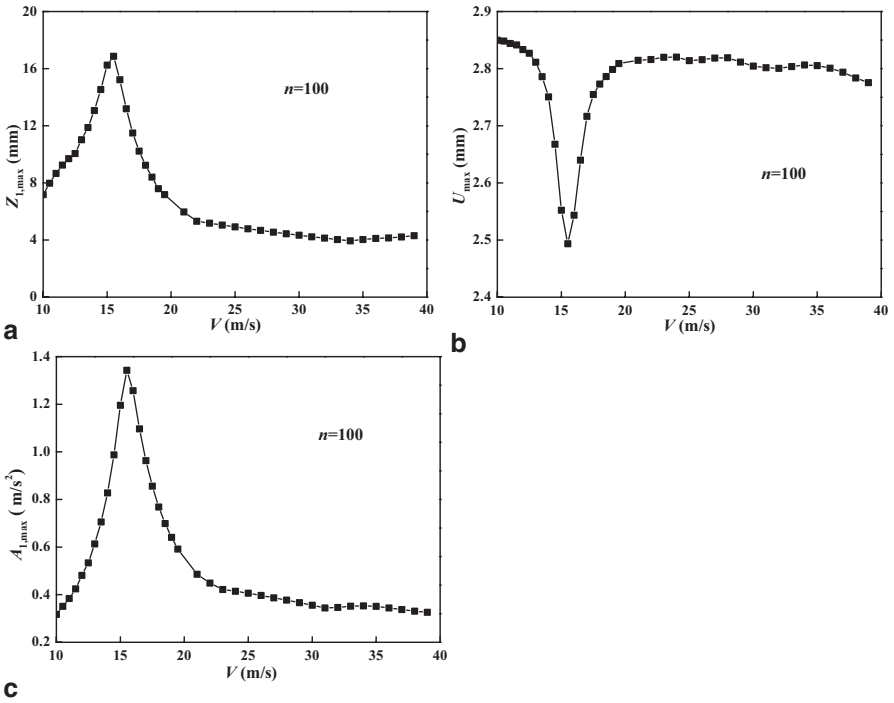

Fig. 4.19 The effects of the speed of the vehicle. (Reprinted from ref. [21], Copyright 2014, with permission from Elsevier)

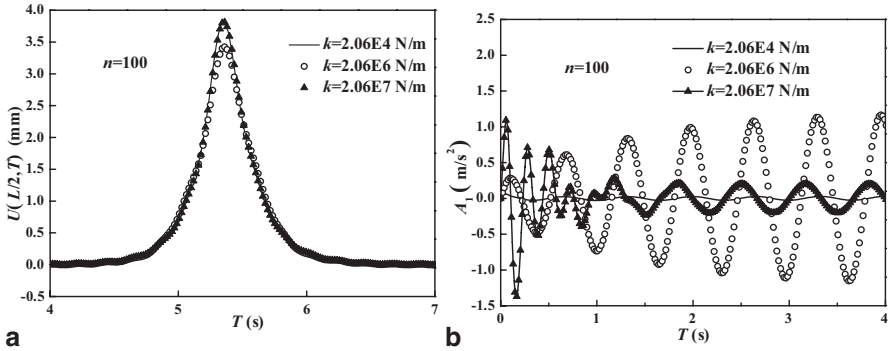

Fig. 4.20 The effects of the suspension stiffness. (Reprinted from ref. [21], Copyright 2014, with permission from Elsevier)

stronger with the decreasing suspension damping. As seen from Fig. 4.21a, the suspension damping has a significant impact on the dynamic response of the pavement. As seen in Figs. 4.18, 4.20 and 4.21 also prove that the dynamic response of the pavement becomes stronger when the vibration of the vehicle becomes weaker.

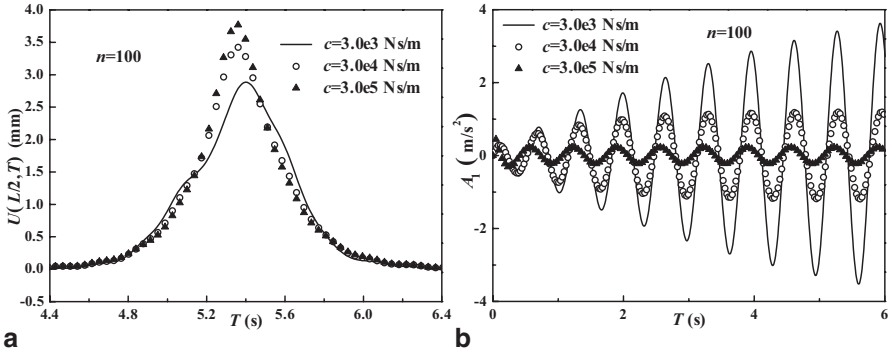

Fig. 4.21 The effects of the suspension damping. (Reprinted from ref. [21], Copyright 2014, with permission from Elsevier)

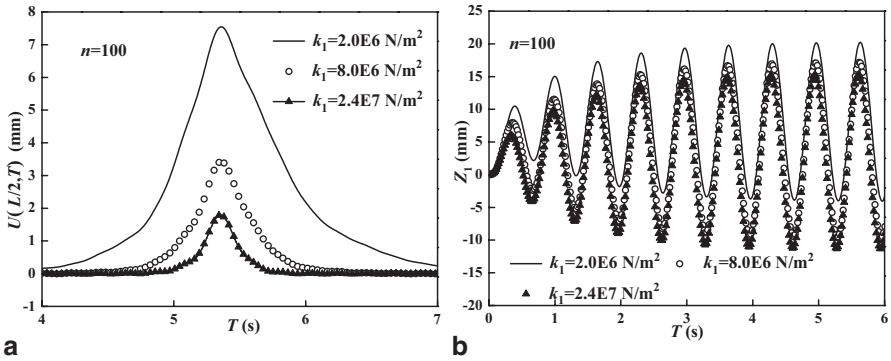

Fig. 4.22 The effects of the linear elastic modulus of the subgrade. (Reprinted from ref. [21], Copyright 2014, with permission from Elsevier)

Physical Parameter Studies

In this section, the effects of the physical parameters of the pavement and the subgrade on the vibration of the vehicle–pavement are investigated by numerical examples. Figure 4.22a and b, respectively, show the effects of the linear elastic modulus of the subgrade on the response of the pavement and the vehicle. The comparison in Fig. 4.22a indicates that the dynamic response of the pavement becomes weaker with the increasing linear elastic modulus of the subgrade. On the other hand, the numerical results in Fig. 4.22b indicate that the parameter of the subgrade changes the response of the pavement faster. The pavement is affected more than the vehicle. Therefore, the authors only show the numerical results of the response of the pavement in the following calculations.

The effects of the other five parameters of the foundation on the dynamic response of the pavement are presented in Fig. 4.23a–e. Meanwhile, the effects of the shear modulus of the pavement are displayed in Fig. 4.23f. Figure 4.23d shows

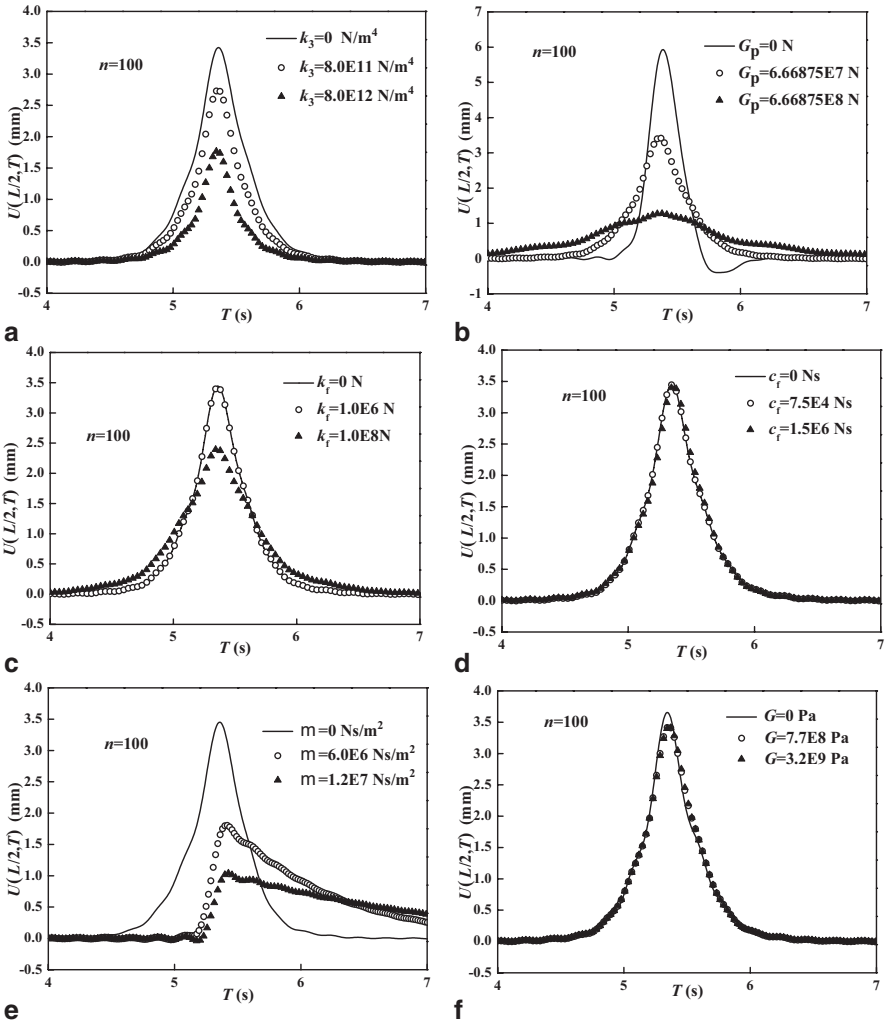

Fig. 4.23 The effects of the physical parameters on the vertical displacements of the pavement's midpoint. (Reprinted from ref. [21], Copyright 2014, with permission from Elsevier)

that the effects of the rocking damping coefficient of the subgrade on the dynamic response of the pavement can be neglected. On the contrary, Fig. 4.23 show that the other five physical parameters, namely, the nonlinear elasticity parameter, the shear deformation coefficient, the rocking stiffness and the damping coefficient of the subgrade, and the shear modulus of the pavement, are all important parameters that influence the dynamic response of the pavement. Furthermore, the response of the pavement decreases with these increasing physical parameters. Therefore, if any of these physical parameters are neglected during the process of modeling, the dynamic analysis overestimates the dynamic response of the pavement.

4.4 The Dynamic Response of an Infinite Timoshenko Beam on a Nonlinear Viscoelastic Foundation [19, 25]

The integral transformation is a powerful tool for dealing with dynamic problems. There are two approaches to deal with a nonlinear term in the governing equations, namely, a perturbation method [26] and the Adomian decomposition method (ADM) without linearization or perturbation [27]. Kargarnovin et al. [26] compared the responses of a nonlinear and an equivalent linear viscoelastic model, and found that the results are completely different at low frequencies. Furthermore, Hryniewicz [27] found that the nonlinearity of the foundation increases the amplitude of vibration under certain conditions. Based on the nonlinear cubic Winkler foundation, Kargarnovin et al. [26] studied the response of an infinite Timoshenko beam subjected to a harmonic moving load, and considered the shear modulus of the beams, without taking into account the shear parameter of the foundation. Hryniewicz [27] discussed the dynamic response of an infinite Rayleigh beam subjected to a moving load without considering the shear modulus of the beam or the foundation. However, there have been no literatures on the dynamic response of an infinite beam on a nonlinear foundation considering the shear deformable beams and shear modulus of the foundation at the same time.

The standard ADM was developed by Adomian for solving linear or nonlinear differential and integral equations [28]. The method has a significant advantage in providing with the solution in a rapid convergent series. Recently several authors have proposed a variety of modifications on the standard ADM. Vahidi and Jalalvand applied the Shanks transformation on the ADM to improve the accuracy of the approximate solutions [29]. Nevertheless, the modified ADM has not been applied to investigate the dynamic response of a beam on a nonlinear foundation.

This section investigates the dynamic response of infinite Timoshenko beams supported by nonlinear viscoelastic foundations to a moving concentrated force. The nonlinearity in the foundation is assumed to be cubic. The nonlinear governing equations of motion are developed by considering the effects of the shear deformable beams and the shear modulus of the foundations at the same time. The differential equations are respectively solved using the ADM and a perturbation method in conjunction with a complex Fourier transformation. An approximate closed form solution is derived in an integral form from the presented Green's function and the theorem of residues, which is used for the calculation of the integral. The dynamic response distribution along the length of the beam is obtained from the closed form solution. The derivation process demonstrates that two methods for the dynamic response of infinite beams on nonlinear foundations to a moving force give a consistent result. The numerical results reveal the influences of the shear deformable beam and the shear modulus of the foundations on dynamic responses. Moreover, the influences on the dynamic response are numerically studied for nonlinearity, viscoelasticity, and other system parameters.

4.4.1 The Mathematical Model

An infinite elastic Timoshenko beam on a nonlinear viscoelastic foundation subjected to a moving load is used to model many engineering devices, as shown in Fig. 4.24, where F_0 and ω are the magnitude and the frequency of the external load, v is the moving speed of the load, t is the time, x is the spatial coordinate along the axis of the beam, $w(X, T)$ is the vertical deflection function of the infinite Timoshenko beam.

The speed of the moving load is assumed to be constant. The nonlinear viscoelastic foundation is taken as a Pasternak foundation with linear-plus-cubic stiffness and viscous damping. Based on these assumptions, the governing differential equations for the displacements $u(x, t)$ and the rotation $\psi(x, t)$ of the beam are

$$\begin{cases} \rho A w_{,TT} + k^* AG\left(\psi_{,X} - w_{,XX}\right) + k_1 w + k_3 w^3 + c w_{,T} - G_p w_{,XX} = F_z\left(X,T\right) \\ \rho I \psi_{,TT} - EI\psi_{,XX} + k^* AG\left(\psi - w_{,X}\right) + k_f \psi + c_f \psi_{,T} = 0 \end{cases} \tag{4.78}$$

where a comma preceding x or t denotes a partial differentiation with respect to x or t, A is the constant cross–section of the homogeneous Timoshenko beam, G, I, ρ, and E are the shear modulus, the second moment of area, the density and the modulus of elasticity of the beam, k^*A is the effective shear area, k_1, k_3, and G_p are the linear, the nonlinear and the shear foundation parameters, c is the damping coefficient of the foundation, k_f and c_f respectively are the rocking stiffness and damping coefficients of the foundation, and the harmonic concentrated moving load is expressed by

$$F_z(X,T) = F_0\, \mathrm{e}^{\mathrm{i}\omega T}\, \delta(X - vT) \tag{4.79}$$

where $\delta(x–vt)$ is the Dirac delta function, which can be defined by

$$\int_{-\infty}^{+\infty} \delta(X - vT) f(X)\, \mathrm{d}X = f(vT) \tag{4.80}$$

for arbitrary function $f(x)$.

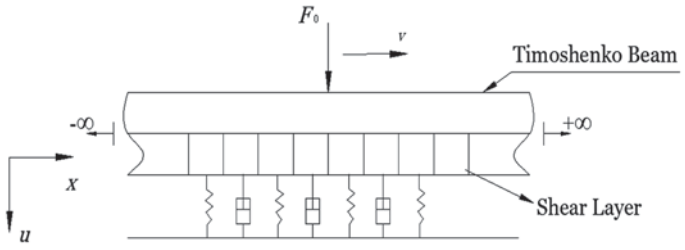

Fig. 4.24 The model of an infinite Timoshenko beam on a nonlinear viscoelastic foundation under a harmonic moving load. (Reprinted from ref. [25], Copyright 2014, with permission from Elsevier)

4.4.2 The Perturbation Method

Introduce a dimensionless variable as follows

$$w(X,T) \leftrightarrow \frac{k_3}{k_1}\sqrt{\frac{I}{A}}w(X,T) \tag{4.81}$$

Substituting Eq. (4.81) into Eq. (4.78) leads to

$$\begin{aligned} &\rho A w_{,TT} + S\psi_{,X} - q w_{,XX} + k_1 w + \varepsilon w^3 + c w_{,T} - G_{\mathrm{p}} w_{,XX} = \frac{F_0 S}{q}\delta(X - vT) \\ &\rho I S\psi_{,TT} - EIS\psi_{,XX} + qS\psi - q^2 w_{,X} + k_{\mathrm{f}} S\psi + c_{\mathrm{f}} S\psi_{,T} = 0 \end{aligned} \tag{4.82}$$

where $q = k^* AG$, $S = q\frac{k_3}{k_1}\sqrt{\frac{I}{A}}$, $\varepsilon = k_3(\frac{q}{S})^2$. Introducing the coordinate transformation

$$\eta = X - vT \tag{4.83}$$

and substituting Eq. (4.83) into Eq. (4.82) yield

$$\begin{aligned} &\left(\rho A v^2 - q - G_{\mathrm{p}}\right)\overline{w}'' - cv\overline{w}' + k_1\overline{w} + \varepsilon\overline{w}^3 + S\overline{\psi}' = \frac{F_0 S}{q}\delta(\eta) \\ &\left(\rho I S v^2 - EIS\right)\overline{\psi}'' - c_{\mathrm{f}} vS\overline{\psi}' + \left(qS + k_{\mathrm{f}} S\right)\overline{\psi} - q^2\overline{w}' = 0 \end{aligned} \tag{4.84}$$

One assumes an expansion of dimensionless displacement

$$\begin{aligned} &\overline{w}(\eta) = \overline{w}_0(\eta) + \overline{w}_1(\eta)\varepsilon + \overline{w}_2(\eta)\varepsilon^2 + \cdots, \\ &\overline{\psi}(\eta) = \overline{\psi}_0(\eta) + \overline{\psi}_1(\eta)\varepsilon + \overline{\psi}_2(\eta)\varepsilon^2 + \cdots \end{aligned} \tag{4.85}$$

Substituting Eq. (4.85) into Eq. (4.84), and then equating coefficient ε^0, ε^1, and ε^2 in the resulting equation, one obtains

$$\varepsilon^0 : F_{\overline{w}0} = \frac{F_0 S}{q}\delta(\eta), F_{\overline{\psi}0} = 0 \tag{4.86}$$

$$\varepsilon^1 : F_{\overline{w}1} = -\overline{w}_0^3, F_{\overline{\psi}1} = 0 \tag{4.87}$$

$$\varepsilon^2 : F_{\overline{w}2} = -3\overline{w}_0^2\overline{w}_1, F_{\overline{\psi}2} = 0 \tag{4.88}$$

where

$$\begin{aligned} F_{\bar{w}k} &= \left(\rho A v^2 - q - G_\mathrm{p}\right)\bar{w}_k'' - cv\bar{w}_k' + k_1\bar{w}_k + S\bar{\psi}_k', \\ F_{\bar{\psi}k} &= \left(\rho I S v^2 - EIS\right)\bar{\psi}_k'' - c_\mathrm{f} v S\bar{\psi}_k' + \left(qS + k_\mathrm{f} S\right)\bar{\psi}_k - q^2\bar{w}_k' \end{aligned} \tag{4.89}$$

$k = 0,1,2$. Then, the application of a complex Fourier transform

$$W_0(\xi) = \int_{-\infty}^{+\infty} \bar{w}_0(\eta)\mathrm{e}^{-\mathrm{i}\eta\xi}\,\mathrm{d}\eta, \Psi_0(\xi) = \int_{-\infty}^{+\infty} \bar{\psi}_0(\eta)\mathrm{e}^{-\mathrm{i}\eta\xi}\,\mathrm{d}\eta \tag{4.90}$$

to Eq. (4.86) leads to

$$\begin{aligned} &\left[\left(-\rho I v^2 + k^* AG + G_\mathrm{p}\right)\xi^2 - \mathrm{i}cv\xi + k_1\right]W_0(\xi) + \mathrm{i}k^* AG\xi\Psi_0(\xi) = F_0, \\ &\left[\left(\rho I v^2 - EI\right)\xi^2 + \mathrm{i}c_\mathrm{f} v\xi - \left(k^* AG + k_\mathrm{f}\right)\right]\Psi_0(\xi) + \mathrm{i}k^* AG\xi W_0(\xi) = 0 \end{aligned} \tag{4.91}$$

$U_0(\xi)$ and $\Psi_0(\xi)$, termed as Green's functions, can be solved from Eq. (4.91)

$$\begin{aligned} W_0(\xi) &= \frac{B_{60}\xi^2 + B_{70}\xi + B_{80}}{B_{10}\xi^4 + B_{20}\xi^3 + B_{30}\xi^2 + B_{40}\xi + B_{50}}, \\ \Psi_0(\xi) &= \frac{\mathrm{i}k^* AGF_0\xi}{B_{10}\xi^4 + B_{20}\xi^3 + B_{30}\xi^2 + B_{40}\xi + B_{50}} \end{aligned} \tag{4.92}$$

where

$$\begin{aligned} B_{10} &= G_\mathrm{p} IE - G_\mathrm{p} v^2\rho I - Av^2 EI\rho + Av^4 I\rho^2 + k^* AGEI - k^* AGv^2\rho I, \\ B_{20} &= -\mathrm{i}vc_\mathrm{f} k^* AG - \mathrm{i}cEIv + \mathrm{i}\rho Icv^3 - \mathrm{i}G_\mathrm{p} vc_\mathrm{f} + \mathrm{i}\rho c_\mathrm{f} v^3 A, \\ B_{30} &= G_\mathrm{p} k^* AG - \rho Av^2 k^* AG + k_\mathrm{f} k^* AG - cc_\mathrm{f} v^2 + EIk_1 - \rho Iv^2 k_1 \\ &\quad + G_\mathrm{p} k_\mathrm{f} - A\rho k_\mathrm{f} v^2, \\ B_{40} &= -\mathrm{i}cvk^* AG - \mathrm{i}vc_\mathrm{f} k_1 - \mathrm{i}cvk_\mathrm{f}, B_{50} = k_1 k^* AG + k_1 k_\mathrm{f}, \\ B_{60} &= EIF_0 - \rho IF_0 v^2, \\ B_{70} &= -\mathrm{i}vc_\mathrm{f} F_0, \\ B_{80} &= F_0 k_\mathrm{f} + F_0 k^* AG \end{aligned} \tag{4.93}$$

Now, if an inverse Fourier transform is taken from both sides of (4.93), then one will get

$$\begin{aligned}\bar{w}_0(\eta) &= \frac{1}{2\pi}\int_{-\infty}^{+\infty} W_0(\xi)\mathrm{e}^{\mathrm{i}\xi\eta}\,\mathrm{d}\xi \\ &= \frac{1}{2\pi}\int_{-\infty}^{+\infty} \frac{B_{60}\xi^2 + B_{70}\xi + B_{80}}{B_{10}\xi^4 + B_{20}\xi^3 + B_{30}\xi^2 + B_{40}\xi + B_{50}}\mathrm{e}^{\mathrm{i}\xi\eta}\,\mathrm{d}\xi \\ \bar{\psi}_0(\eta) &= \frac{1}{2\pi}\int_{-\infty}^{+\infty} \Psi_0(\xi)\mathrm{e}^{\mathrm{i}\xi\eta}\,\mathrm{d}\xi \\ &= \frac{1}{2\pi}\int_{-\infty}^{+\infty} \frac{\mathrm{i}k^* AGF_0\xi}{B_{10}\xi^4 + B_{20}\xi^3 + B_{30}\xi^2 + B_{40}\xi + B_{50}}\mathrm{e}^{\mathrm{i}\xi\eta}\,\mathrm{d}\xi\end{aligned} \tag{4.94}$$

To calculate the integrals of Eq. (4.94), it is necessary to employ the residue theorem. According to the residue theorem, the integrals of Eq. (4.94) are returned to the sum of the residues at the poles. The poles are the roots of $B_{10}\xi^4 + B_{20}\xi^3 + B_{30}\xi^2 + B_{40}\xi + B_{50} = 0$. Since the beam length is considered to be infinite, the boundary conditions are

$$\lim_{\eta\to\pm\infty}\bar{w} = \lim_{\eta\to\pm\infty}\bar{w}' = \lim_{\eta\to\pm\infty}\bar{w}'' = 0,\ \lim_{\eta\to\pm\infty}\bar{\psi} = \lim_{\eta\to\pm\infty}\bar{\psi}' = \lim_{\eta\to\pm\infty}\bar{\psi}'' = 0 \tag{4.95}$$

The closed form solutions are obtained as

$$\begin{aligned}\bar{w}_0(\eta) &= \frac{1}{2\pi}\mathrm{Re}\,s\left\{\frac{B_{60}\xi^2 + B_{70}\xi + B_{80}}{B_{10}\xi^4 + B_{20}\xi^3 + B_{30}\xi^2 + B_{40}\xi + B_{50}}\mathrm{e}^{\mathrm{i}\xi\eta}\right\}\Bigg|_{\xi=\xi_l} \\ &= \frac{1}{2\pi}\left[2\pi\mathrm{i}\sum_{\mathrm{Im}\,\xi_j>0}\lim_{\xi\to\xi_j}(\xi-\xi_j)W_0(\xi)\mathrm{e}^{\mathrm{i}\xi\eta} + \pi\mathrm{i}\sum_{\mathrm{Im}\,\xi_j=0}\lim_{\xi\to\xi_j}(\xi-\xi_j)W_0(\xi)\mathrm{e}^{\mathrm{i}\xi\eta}\right] \\ \bar{\psi}_0(\eta) &= \frac{1}{2\pi}\mathrm{Re}\,s\left\{\frac{\mathrm{i}k^* AGF_0\xi}{B_{10}\xi^4 + B_{20}\xi^3 + B_{30}\xi^2 + B_{40}\xi + B_{50}}\mathrm{e}^{\mathrm{i}\xi\eta}\right\}\Bigg|_{\xi=\xi_l} \\ &= \frac{1}{2\pi}\left[2\pi\mathrm{i}\sum_{\mathrm{Im}\,\xi_j>0}\lim_{\xi\to\xi_j}(\xi-\xi_j)\Psi_0(\xi)\mathrm{e}^{\mathrm{i}\xi\eta} + \pi\mathrm{i}\sum_{\mathrm{Im}\,\xi_j=0}\lim_{\xi\to\xi_j}(\xi-\xi_j)\Psi_0(\xi)\mathrm{e}^{\mathrm{i}\xi\eta}\right]\end{aligned} \tag{4.96}$$

for $\eta \geq 0$, where ξ_j in the first part of Eq. (4.96) is the pole of $W_0(\xi)$ in the upper half part of the complex plane and ξ_j in the second part of Eq. (4.96) is the pole of $\Psi_0(\xi)$ in the upper half part of the complex plane, and

$$\begin{aligned}
\bar{w}_0(\eta) &= \frac{1}{2\pi}\mathrm{Re}\,s\left\{\frac{B_{60}\xi^2+B_{70}\xi+B_{80}}{B_{10}\xi^4+B_{20}\xi^3+B_{30}\xi^2+B_{40}\xi+B_{50}}\mathrm{e}^{\mathrm{i}\xi\eta}\right\}\Bigg|_{\xi=\xi_l} \\
&= \frac{1}{2\pi}\left[-2\pi\mathrm{i}\sum_{\mathrm{Im}\,\xi_j<0}\lim_{\xi\to\xi_j}(\xi-\xi_j)W_0(\xi)\mathrm{e}^{\mathrm{i}\xi\eta}-\pi\mathrm{i}\sum_{\mathrm{Im}\,\xi_j=0}\lim_{\xi\to\xi_j}(\xi-\xi_j)W_0(\xi)\mathrm{e}^{\mathrm{i}\xi\eta}\right] \\
\bar{\psi}_0(\eta) &= \frac{1}{2\pi}\mathrm{Re}\,s\left\{\frac{\mathrm{i}k^*AGF_0\xi}{B_{10}\xi^4+B_{20}\xi^3+B_{30}\xi^2+B_{40}\xi+B_{50}}\mathrm{e}^{\mathrm{i}\xi\eta}\right\}\Bigg|_{\xi=\xi_l} \\
&= \frac{1}{2\pi}\left[-2\pi\mathrm{i}\sum_{\mathrm{Im}\,\xi_j<0}\lim_{\xi\to\xi_j}(\xi-\xi_j)\Psi_0(\xi)\mathrm{e}^{\mathrm{i}\xi\eta}-\pi\mathrm{i}\sum_{\mathrm{Im}\,\xi_j=0}\lim_{\xi\to\xi_j}(\xi-\xi_j)\Psi_0(\xi)\mathrm{e}^{\mathrm{i}\xi\eta}\right]
\end{aligned} \tag{4.97}$$

for $\eta \le 0$, where ξ_j in the first part of Eq. (4.97) is the pole of $W_0(\xi)$ in the lower half part of the complex plane and ξ_j in the second part of Eq. (4.97) is the pole of $\Psi_0(\xi)$ in the lower half part of the complex plane.

When the integrals of Eq. (4.94) have high order poles, the closed form solutions are obtained as

$$\begin{aligned}
\bar{w}_0(\eta) &= \frac{1}{2\pi}\mathrm{Res}\left\{\frac{B_{60}\xi^2+B_{70}\xi+B_{80}}{B_{10}\xi^4+B_{20}\xi^3+B_{30}\xi^2+B_{40}\xi+B_{50}}\mathrm{e}^{\mathrm{i}\xi\eta}\right\}\Bigg|_{\xi=\xi_l} \\
&= \frac{1}{2\pi}\lim_{\xi\to\xi_l}\frac{\mathrm{d}}{\mathrm{d}\xi}\left\{\frac{B_{60}\xi^2+B_{70}\xi+B_{80}}{(\xi-\xi_1)(\xi-\xi_2)}\mathrm{e}^{\mathrm{i}\xi\eta}\right\} \\
\bar{\psi}_0(\eta) &= \frac{1}{2\pi}\mathrm{Res}\left\{\frac{\mathrm{i}k^*AGF_0\xi}{B_{10}\xi^4+B_{20}\xi^3+B_{30}\xi^2+B_{40}\xi+B_{50}}\mathrm{e}^{\mathrm{i}\xi\eta}\right\}\Bigg|_{\xi=\xi_l} \\
&= \frac{1}{2\pi}\lim_{\xi\to\xi_l}\frac{\mathrm{d}}{\mathrm{d}\xi}\left\{\frac{\mathrm{i}k^*AGF_0\xi}{(\xi-\xi_1)(\xi-\xi_2)}\mathrm{e}^{\mathrm{i}\xi\eta}\right\}
\end{aligned} \tag{4.98}$$

where ξ_l in the first part of Eq. (4.98) is the second order pole of $U_0(\xi)$, ξ_1 and ξ_2 are the first order poles. ξ_l in the second part of Eq. (4.98) is the second order pole of $\Psi_0(\xi)$, ξ_1 and ξ_2 are the first order poles.

Using a similar procedure based on appropriate Green's functions and the convolution integral theorem, one obtains the closed form solutions

$$\begin{aligned}
\bar{w}_1(\eta) &= -\int_{-\infty}^{+\infty}\bar{w}_0^3(\eta-\eta^*)\tilde{w}_1(\eta^*)\mathrm{d}\eta^*, \\
\bar{\psi}_1(\eta) &= -\int_{-\infty}^{+\infty}\bar{w}_0^3(\eta-\eta^*)\tilde{\psi}_1(\eta^*)\mathrm{d}\eta^*
\end{aligned} \tag{4.99}$$

$$\begin{aligned}
\bar{w}_2(\eta) &= -3\int_{-\infty}^{+\infty}\bar{w}_0^2(\eta-\eta^*)\bar{w}_1(\eta-\eta^*)\tilde{w}_1(\eta^*)\mathrm{d}\eta^*, \\
\bar{\psi}_2(\eta) &= -3\int_{-\infty}^{+\infty}\bar{w}_0^2(\eta-\eta^*)\bar{w}_1(\eta-\eta^*)\tilde{\psi}_1(\eta^*)\mathrm{d}\eta^*
\end{aligned} \tag{4.100}$$

where $\tilde{w}_1(\eta)$ and $\tilde{\psi}_1(\eta)$ can be determined by

$$\begin{aligned} L_1\tilde{w}_1(\eta)+L_2\tilde{\psi}_1(\eta)&=\delta(\eta)\\ -L_2\tilde{w}_1(\eta)+L_3\tilde{\psi}_1(\eta)&=0 \end{aligned} \tag{4.101}$$

Therefore, the dynamic response of the system can be determined by the following equation

$$\bar{w}(\eta)=\bar{w}_0(\eta)+\bar{w}_1(\eta)+\bar{w}_2(\eta) \tag{4.102}$$

The same procedure is applicable in the case of Euler–Bernoulli beams. In this case, the equations of motion can be derived as

$$EIw_{,XXXX}+\rho Aw_{,TT}-G_pw_{,XX}+k_1w+k_3w^3+cw_{,T}=F_0\delta(X-vT) \tag{4.103}$$

Using the same procedure, one can calculate the closed form solution as

$$\begin{aligned} \bar{w}_0(\eta)&=\frac{F_0}{2\pi}\int_{-\infty}^{+\infty}\frac{\mathrm{e}^{\mathrm{i}\xi\eta}}{EI\xi^4+\left(G_\mathrm{p}-\rho Av^2\right)\xi^2-\mathrm{i}cv\xi+k_1}\mathrm{d}\xi,\\ \bar{w}_1(\eta)&=-\int_{-\infty}^{+\infty}\bar{w}_0^3\left(\eta-\eta^*\right)\tilde{w}_1(\eta^*)\mathrm{d}\eta^*\\ \bar{w}_2(\eta)&=-3\int_{-\infty}^{+\infty}\bar{w}_0^2\left(\eta-\eta^*\right)\bar{w}_1\left(\eta-\eta^*\right)\tilde{w}_1\left(\eta^*\right)\mathrm{d}\eta^* \end{aligned} \tag{4.104}$$

Using the same method of the residue theorem, one will solve Eq. (4.104).

4.4.3 The Modified ADM

The ADM is an iterative method, which has proven successful in dealing with nonlinear equations. This method is based on the search for a solution in the form of a series in which the nonlinear terms are calculated recursively using the Adomian polynomials. The main properties of the method are that it is capable of reducing the size of computational work while still maintaining highly accurate numerical solutions. In this study, a moving harmonic load is considered, and the modified ADM is used to deal with the nonlinear term of the foundation reaction. The complex integral transformations, Green's function, and the theorem of residues are employed for the dynamic response of the Timoshenko beam with an infinite length supported by a nonlinear foundation.

The ADM gives the solutions $u(x, t)$ and $\psi(x, t)$ of Eq. (4.78) in a series form of the infinite sum

$$\begin{aligned} w(X,T)&=\sum_{j=0}^{+\infty}w_j(X,T),\\ \psi(X,T)&=\sum_{j=0}^{+\infty}\psi_j(X,T) \end{aligned} \tag{4.105}$$

Substitution of Eq. (4.105) into the linear terms in Eq. (4.78) yields

$$\begin{aligned} &L_1\sum_{j=0}^{+\infty} w_j\left(X,T\right)+L_2\sum_{j=0}^{+\infty}\psi_j\left(X,T\right)=F_0\,\mathrm{e}^{\mathrm{i}\omega T}\,\delta\left(X-vT\right)-k_3 f\left(w\right)\\ &-L_2\sum_{j=0}^{+\infty} w_j\left(X,T\right)+L_3\sum_{j=0}^{+\infty}\psi_j\left(X,T\right)=0 \end{aligned} \tag{4.106}$$

where $f(w)$ and L_i $(i=1,2,3)$ are called the nonlinear operator and the linear operator and defined by

$$f(w)=w^3 \tag{4.107}$$

$$\begin{aligned} L_1&=\rho A\frac{\partial}{\partial T^2}-k^* AG\frac{\partial}{\partial X^2}+c\frac{\partial}{\partial T}-G_{\mathrm{p}}\frac{\partial}{\partial X^2}+k_1,\\ L_2&=k^* AG\frac{\partial}{\partial X},\\ L_3&=\rho I\frac{\partial}{\partial T^2}-EI\frac{\partial}{\partial X^2}+c_{\mathrm{f}}\frac{\partial}{\partial T}+k^* AG+k_{\mathrm{f}} \end{aligned} \tag{4.108}$$

In order to solve Eq. (4.106) via the ADM, the nonlinear operator $f(w)$ can be decomposed into the form of the infinite sum of series

$$f(w)=\sum_{j=0}^{+\infty}\overline{A}_j \tag{4.109}$$

where $\overline{A}_j$ are called Adomian polynomials of $w_1, w_2, \ldots, w_j$. So that Eq. (4.106) is rewritten as the recursive form

$$\begin{aligned} &L_1 w_0\left(X,T\right)+L_2\psi_0\left(X,T\right)=F_0\,\mathrm{e}^{\mathrm{i}\omega T}\,\delta\left(X-vT\right)\\ &-L_2 w_0\left(X,T\right)+L_3\psi_0\left(X,T\right)=0 \end{aligned} \tag{4.110}$$

for $j=0$, and

$$\begin{aligned} &L_1 w_j\left(X,T\right)+L_2\psi_j\left(X,T\right)=-k_3\overline{A}_{j-1}\\ &-L_2 w_j\left(X,T\right)+L_3\psi_j\left(X,T\right)=0 \end{aligned} \tag{4.111}$$

for $j\geq 1$.

The modified ADM suggests that the nonlinear operator $f(w)$ can be decomposed by the following polynomials

$$
\begin{aligned}
&\overline{A}_0 = f(w_0) = w_0^3 \\
&\overline{A}_1 = w_1 \frac{\mathrm{d}f(w_0)}{\mathrm{d}w_0} + \frac{1}{2!} w_1^2 \frac{\mathrm{d}^2 f(w_0)}{\mathrm{d}w_0^2} + \frac{1}{3!} w_1^3 \frac{\mathrm{d}^3 f(w_0)}{\mathrm{d}w_0^3} + \cdots \\
&\overline{A}_2 = w_2 \frac{\mathrm{d}f(w_0)}{\mathrm{d}w_0} + \frac{w_1^2}{2!}\left(w_2^2 + 2w_1 w_2\right) \frac{\mathrm{d}^2 f(w_0)}{\mathrm{d}w_0^2} + \frac{1}{3!}\left(3\left(w_1^2 w_2 + w_1 w_2^2\right) + w_2^3\right) \frac{\mathrm{d}^3 f(w_0)}{\mathrm{d}w_0^3} + \cdots \\
&\overline{A}_3 = w_3 \frac{\mathrm{d}f(w_0)}{\mathrm{d}w_0} + \frac{1}{2!}(w_3^2 + 2w_1 w_3 + 2w_2 w_3) \frac{\mathrm{d}^2 f(w_0)}{\mathrm{d}w_0^2} + \frac{1}{3!}\Big[w_1^3 + 3w_3^2\left(w_1 + w_2\right) \\
&\quad + 3w_3\left(w_1 + w_2\right)^2\Big] \frac{\mathrm{d}^3 f(w_0)}{\mathrm{d}w_0^3} + \cdots \\
&\quad \vdots
\end{aligned}
\tag{4.112}
$$

So here $\overline{A}_j$ are given as

$$
\begin{aligned}
&\overline{A}_0 = w_0^3, \\
&\overline{A}_1 = 3w_0^2 w_1 + w_1^2 w_0 + w_1^3, \\
&\vdots
\end{aligned}
\tag{4.113}
$$

Since the beam is infinitely long and the transverse load moves in the positive x direction with a constant velocity v, a moving coordinate η can be defined by

$$
\eta = x - vt \tag{4.114}
$$

For an infinite Timoshenko beam in the steady-state dynamic response, one can assume the form of the solution for (4.110) as

$$
\begin{aligned}
w_0(X,T) &= \overline{w}_0(\eta) = \tilde{w}_0(\eta)\mathrm{e}^{\mathrm{i}\omega T}, \\
\psi_0(X,T) &= \overline{\psi}_0(\eta) = \tilde{\psi}_0(\eta)\mathrm{e}^{\mathrm{i}\omega T}
\end{aligned}
\tag{4.115}
$$

The following results can be obtained

$$
\begin{aligned}
&w_{0,T} = \left(-v\tilde{w}_0' + \mathrm{i}\omega\tilde{w}_0\right)\mathrm{e}^{\mathrm{i}\omega T}, \\
&w_{0,TT} = \left(v^2\tilde{w}_0'' - 2\mathrm{i}\omega v\tilde{w}_0' - \omega^2 w_0\right)\mathrm{e}^{\mathrm{i}\omega T}, \\
&w_{0,T} = \tilde{w}_0'\mathrm{e}^{\mathrm{i}\omega T}, \\
&w_{0,TT} = \tilde{w}_0''\mathrm{e}^{\mathrm{i}\omega T} \\
&\psi_{0,T} = \left(-v\tilde{\psi}_0' + \mathrm{i}\omega\tilde{\psi}_0\right)\mathrm{e}^{\mathrm{i}\omega T}, \\
&\psi_{0,TT} = \left(v^2\tilde{\psi}_0'' - 2\mathrm{i}\omega v\tilde{\psi}_0' - \omega^2\psi_0\right)\mathrm{e}^{\mathrm{i}\omega T}, \\
&\psi_{0,X} = \tilde{\psi}_0'\mathrm{e}^{\mathrm{i}\omega T}, \psi_{0,XX} = \tilde{\psi}_0''\mathrm{e}^{\mathrm{i}\omega T}
\end{aligned}
\tag{4.116}
$$

where the prime indicates differentiation with respect to η. Substitution of Eq. (4.116) into Eq. (4.110) yields

$$\begin{aligned}
&\left(\rho Av^2 - k^* AG - G_\mathrm{p}\right)\tilde{w}_0'' + \left(-2\mathrm{i}\omega v\rho A - cv\right)\tilde{w}_0' + \left(-\omega^2\rho A + k_1 + \mathrm{i}c\omega\right)\tilde{w}_0 \\
&\qquad + k^* AG\tilde{\psi}_0' = F_0\delta(\eta) \\
&\left(\rho Iv^2 - EI\right)\tilde{\psi}_0'' + \left(-2\mathrm{i}\omega v\rho I - vc_\mathrm{f}\right)\tilde{\psi}_0' + \left(-\omega^2\rho I + k^* AG + k_\mathrm{f} + \mathrm{i}\omega c_\mathrm{f}\right)\tilde{\psi}_0 \\
&\qquad - k^* AG\tilde{w}_0' = 0
\end{aligned} \tag{4.117}$$

Considering the boundary conditions of an infinite beam and applying the complex Fourier transform to (4.117), one will get

$$\begin{aligned}
W_0(\xi) &= \int_{-\infty}^{+\infty} \tilde{w}_0(\eta)\mathrm{e}^{-\mathrm{i}\eta\xi}\,\mathrm{d}\eta = \frac{B_{60}\xi^2 + B_{70}\xi + B_{80}}{B_{10}\xi^4 + B_{20}\xi^3 + B_{30}\xi^2 + B_{40}\xi + B_{50}}, \\
\Psi_0(\xi) &= \int_{-\infty}^{+\infty} \tilde{\psi}_0(\eta)\mathrm{e}^{-\mathrm{i}\eta\xi}\,\mathrm{d}\eta = \frac{-\mathrm{i}k^* AGF_0\xi}{B_{10}\xi^4 + B_{20}\xi^3 + B_{30}\xi^2 + B_{40}\xi + B_{50}}
\end{aligned} \tag{4.118}$$

where $W_0(\xi)$ and $\tilde{w}_0(\eta)$ are a couple of Fourier transforms, $\Psi_0(\xi)$ and $\tilde{\psi}_0(\eta)$ are also a couple of Fourier transforms. $B_{10} - B_{80}$ are determined by the following terms

$$\begin{aligned}
B_{10} &= -G_\mathrm{p}IE + G_\mathrm{p}v^2\rho I + Av^2EI\rho - Av^4I\rho^2 - k^* AGEI + k^* AGv^2\rho I, \\
B_{20} &= \mathrm{i}cEIv - \mathrm{i}\rho Icv^3 - 2G_\mathrm{p}v\omega\rho I - 2Av\omega EI\rho + 4Av^3\omega\rho^2 I + \mathrm{i}G_\mathrm{p}vc_\mathrm{f} \\
&\quad - \mathrm{i}\rho c_\mathrm{f}v^3 A - 2AG\omega\rho Ik^* + \mathrm{i}vc_\mathrm{f}k^* AG, \\
B_{30} &= -\mathrm{i}c\omega EI + 3Icv^2\omega\rho I + G_\mathrm{p}\omega^2\rho I + A\omega^2 EI\rho - 6Av^2\omega^2 I\rho^2 + cc_\mathrm{f}v^2 - \mathrm{i}G_\mathrm{p}\omega c_\mathrm{f} \\
&\quad + 3\mathrm{i}Av^2\omega\rho c_\mathrm{f} - EIk_1 + \rho Iv^2k_1 - G_\mathrm{p}k_\mathrm{f} + \rho Av^2k_\mathrm{f} - G_\mathrm{p}k^* AG + A^2Gv^2\rho k^* \\
&\quad + AG\omega^2\rho Ik^* - \mathrm{i}AG\omega c_\mathrm{f}k^* - AGk_\mathrm{f}k^*, \\
B_{40} &= -3\mathrm{i}cv\omega^2\rho I + 4Av\omega^3 I\rho^2 - 2cv\omega c_\mathrm{f} - 3\mathrm{i}Av\omega^2\rho c_\mathrm{f} - 2v\omega I\rho k_1 \\
&\quad + \mathrm{i}vc_\mathrm{f}k_1 + \mathrm{i}cvk_\mathrm{f} - 2Av\omega\rho k_\mathrm{f} + \mathrm{i}AcGvk^* - 2A^2Gv\omega\rho k_1, \\
B_{50} &= -k_1k^* AG - k_1k_\mathrm{f} + \mathrm{i}c\omega^3 I\rho - A\omega^4 I\rho^2 + c\omega^2 c_\mathrm{f} + \mathrm{i}A\omega^3\rho c_\mathrm{f} + \omega^2 I\rho k_1 - \mathrm{i}\omega c_\mathrm{f}k_1 \\
&\quad - \mathrm{i}c\omega k_\mathrm{f} + A\omega^2\rho k_\mathrm{f} - \mathrm{i}AcG\omega k^* + A^2G\omega^2\rho k^*, \\
B_{60} &= -EIF_0 + \rho IF_0v^2, \\
B_{70} &= -2v\omega I\rho F_0 + \mathrm{i}vc_\mathrm{f}F_0, \\
B_{80} &= \omega^2 I\rho F_0 - \mathrm{i}\omega c_\mathrm{f}F_0 - F_0k_\mathrm{f} - F_0k^* AG
\end{aligned} \tag{4.119}$$

Now, if an inverse Fourier transform is taken from both sides of Eq. (4.119), then one will get

$$\tilde{w}_0(\eta)=\frac{1}{2\pi}\int_{-\infty}^{+\infty}\frac{B_{60}\xi^2+B_{70}\xi+B_{80}}{B_{10}\xi^4+B_{20}\xi^3+B_{30}\xi^2+B_{40}\xi+B_{50}}\mathrm{e}^{\mathrm{i}\xi\eta}\,\mathrm{d}\,\xi \tag{4.120}$$

$$\tilde{\psi}_0(\eta)=\frac{1}{2\pi}\int_{-\infty}^{+\infty}\frac{-\mathrm{i}k^*AGF_0\xi}{B_{10}\xi^4+B_{20}\xi^3+B_{30}\xi^2+B_{40}\xi+B_{50}}\mathrm{e}^{\mathrm{i}\xi\eta}\,\mathrm{d}\,\xi$$

Equation (4.120) can be calculated via employing the residue theorem. According to the residue theorem, the integrals of Eq. (4.120) are the sum of residues at the poles. The poles are the roots of the denominator in Eq. (4.120). The closed form solutions are obtained as

$$\begin{aligned}\tilde{w}_0(\eta)&=\mathrm{i}\sum_{\mathrm{Im}\,\xi_j>0}\lim_{\xi\to\xi_j}\frac{(\xi-\xi_j)\left(B_{60}\xi^2+B_{70}\xi+B_{80}\right)}{B_{10}\xi^4+B_{20}\xi^3+B_{30}\xi^2+B_{40}\xi+B_{50}}\mathrm{e}^{\mathrm{i}\xi\eta}\\&\quad+\frac{\mathrm{i}}{2}\sum_{\mathrm{Im}\,\xi_j=0}\lim_{\xi\to\xi_j}\frac{(\xi-\xi_j)\left(B_{60}\xi^2+B_{70}\xi+B_{80}\right)}{B_{10}\xi^4+B_{20}\xi^3+B_{30}\xi^2+B_{40}\xi+B_{50}}\mathrm{e}^{\mathrm{i}\xi\eta}\\\tilde{\psi}_0(\eta)&=\mathrm{i}\sum_{\mathrm{Im}\,\xi_n>0}\lim_{\xi\to\xi_n}\frac{(\xi-\xi_n)\left(-\mathrm{i}k^*AGF_0\xi\right)}{B_{10}\xi^4+B_{20}\xi^3+B_{30}\xi^2+B_{40}\xi+B_{50}}\mathrm{e}^{\mathrm{i}\xi\eta}\\&\quad+\frac{\mathrm{i}}{2}\sum_{\mathrm{Im}\,\xi_n=0}\lim_{\xi\to\xi_n}\frac{(\xi-\xi_n)\left(-\mathrm{i}k^*AGF_0\xi\right)}{B_{10}\xi^4+B_{20}\xi^3+B_{30}\xi^2+B_{40}\xi+B_{50}}\mathrm{e}^{\mathrm{i}\xi\eta}\end{aligned} \tag{4.121}$$

for $\eta\geq 0$, where ξ_j and ξ_n are the poles of $W_0(\xi)$ and $\Psi_0(\xi)$ in the upper half part of the complex plane, and

$$\begin{aligned}\tilde{w}_0(\eta)&=\mathrm{i}\sum_{\mathrm{Im}\,\xi_j<0}\lim_{\xi\to\xi_j}\frac{(\xi-\xi_j)\left(B_{60}\xi^2+B_{70}\xi+B_{80}\right)}{B_{10}\xi^4+B_{20}\xi^3+B_{30}\xi^2+B_{40}\xi+B_{50}}\mathrm{e}^{\mathrm{i}\xi\eta}\\&\quad+\frac{\mathrm{i}}{2}\sum_{\mathrm{Im}\,\xi_j=0}\lim_{\xi\to\xi_j}\frac{(\xi-\xi_j)\left(B_{60}\xi^2+B_{70}\xi+B_{80}\right)}{B_{10}\xi^4+B_{20}\xi^3+B_{30}\xi^2+B_{40}\xi+B_{50}}\mathrm{e}^{\mathrm{i}\xi\eta}\\\tilde{\psi}_0(\eta)&=\mathrm{i}\sum_{\mathrm{Im}\,\xi_n<0}\lim_{\xi\to\xi_n}\frac{(\xi-\xi_n)\left(-\mathrm{i}k^*AGF_0\xi\right)}{B_{10}\xi^4+B_{20}\xi^3+B_{30}\xi^2+B_{40}\xi+B_{50}}\mathrm{e}^{\mathrm{i}\xi\eta}\\&\quad+\frac{\mathrm{i}}{2}\sum_{\mathrm{Im}\,\xi_n=0}\lim_{\xi\to\xi_n}\frac{(\xi-\xi_n)\left(-\mathrm{i}k^*AGF_0\xi\right)}{B_{10}\xi^4+B_{20}\xi^3+B_{30}\xi^2+B_{40}\xi+B_{50}}\mathrm{e}^{\mathrm{i}\xi\eta}\end{aligned} \tag{4.122}$$

for $\eta\leq 0$, where ξ_j and ξ_n are the poles of $w_0(\xi)$ and $\Psi_0(\xi)$ in the lower half part of the complex plane. When the integrals of Eq. (4.120) have high order poles, the sum of residues at the poles are obtained as

$$\operatorname{Res}\left\{\frac{B_{60}\xi^2+B_{70}\xi+B_{80}}{B_{10}\xi^4+B_{20}\xi^3+B_{30}\xi^2+B_{40}\xi+B_{50}}\mathrm{e}^{\mathrm{i}\xi\eta}\right\}\Bigg|_{\xi=\xi_l}\lim_{\xi\to\xi_l}\frac{\mathrm{d}}{\mathrm{d}\xi}\left\{\frac{B_{60}\xi^2+B_{70}\xi+B_{80}}{(\xi-\xi_1)(\xi-\xi_2)}\mathrm{e}^{\mathrm{i}\xi\eta}\right\}$$
$$\operatorname{Res}\left\{\frac{\mathrm{i}k'AGF_0\xi}{B_{10}\xi^4+B_{20}\xi^3+B_{30}\xi^2+B_{40}\xi+B_{50}}\mathrm{e}^{\mathrm{i}\xi\eta}\right\}\Bigg|_{\xi=\xi_m}=\lim_{\xi\to\xi_m}\frac{\mathrm{d}}{\mathrm{d}\xi}\left\{\frac{\mathrm{i}k'AGF_0\xi}{(\xi-\xi_1)(\xi-\xi_2)}\mathrm{e}^{\mathrm{i}\xi\eta}\right\} \tag{4.123}$$

where ξ_l and ξ_m are the second order poles of $w_0(\xi)$ and $\Psi_0(\xi)$, respectively, ξ_1 and ξ_2 are the first order poles.

As pointed out by Wazwaz [30], the modified decomposition method may give the exact solution for nonlinear equations by only using two iterations. In the following computations, the infinite series $\overline{A}_j$ only keeps the first three terms for the modified ADM. Now, consider Eq. (4.111). For $j=1$ and 2, Eq. (4.111) can be rewritten as

$$\begin{aligned}&\left(\rho Av^2-k^*AG-G_\mathrm{p}\right)\tilde{w}_1''-cv\tilde{w}_1'+k_1\tilde{w}_1+k^*AG\tilde{\psi}_1'=-k_3\tilde{w}_0^3\\&\left(\rho Iv^2-EI\right)\tilde{\psi}_1''-c_\mathrm{f}v\tilde{\psi}_1'+\left(k^*AG+k_\mathrm{f}\right)\tilde{\psi}_1-k^*AG\tilde{w}_1'=0\end{aligned} \tag{4.124}$$

and

$$\begin{aligned}&\left(\rho AV^2-k^*AG-G_\mathrm{p}\right)\tilde{w}_2''-cV\tilde{w}_2'+k_1\tilde{w}_2+k^*AG\tilde{\psi}_2'=-3k_3\tilde{w}_0^2\tilde{w}_1-3k_3\tilde{w}_1^2\tilde{w}_0-k_3\tilde{w}_1^3\\&\left(\rho IV^2-EI\right)\tilde{\psi}_2''-c_\mathrm{f}V\tilde{\psi}_2'+\left(k^*AG+k_\mathrm{f}\right)\tilde{\psi}_2-k^*AG\tilde{w}_2'=0\end{aligned} \tag{4.125}$$

Using a similar procedure for Eq. (4.117) and the convolution integral theorem, one obtains the closed form solutions of Eqs. (4.124) and (4.125)

$$\begin{aligned}\tilde{w}_1(\eta)&=-k_3\int_{-\infty}^{+\infty}\tilde{w}_0^3\left(\eta-\eta^*\right)\hat{w}_{11}\left(\eta^*\right)\mathrm{d}\eta^*,\\\tilde{\psi}_1(\eta)&=-k_3\int_{-\infty}^{+\infty}\tilde{w}_0^3\left(\eta-\eta^*\right)\bar{\psi}_{11}\left(\eta^*\right)\mathrm{d}\eta^*\end{aligned} \tag{4.126}$$

and

$$\begin{aligned}\tilde{w}_2(\eta)&=-k_3\int_{-\infty}^{+\infty}\left[3\tilde{w}_0^2\left(\eta-\eta^*\right)\tilde{w}_1\left(\eta-\eta^*\right)+3\tilde{w}_1^2\left(\eta-\eta^*\right)\tilde{w}_0\left(\eta-\eta^*\right)+\tilde{w}_1^3\left(\eta-\eta^*\right)\right]\hat{w}_{21}\left(\eta^*\right)\mathrm{d}\eta^*,\\\tilde{\psi}_2(\eta)&=-k_3\int_{-\infty}^{+\infty}\left[3\tilde{w}_0^2\left(\eta-\eta^*\right)\tilde{w}_1\left(\eta-\eta^*\right)+3\tilde{w}_1^2\left(\eta-\eta^*\right)\tilde{w}_0\left(\eta-\eta^*\right)+\tilde{w}_1^3\left(\eta-\eta^*\right)\right]\bar{\psi}_{21}\left(\eta^*\right)\mathrm{d}\eta^*\end{aligned} \tag{4.127}$$

where $\hat{w}_{j1}(\eta)$ and $\bar{\psi}_{j1}(\eta)$ ($j=1, 2$) are the dynamic responses of $\mathrm{e}^{i\omega_j T}\,\delta(X-vT)$, $\omega_1=3\omega$ and $\omega_2=5\omega$. Using the same method of the residue theorem, the Eqs. (4.126) and (4.127) will be solved. According to the procedure for solving Eq. (4.117), $B_{1j}-B_{8j}$ are determined by the following terms

$$
\begin{aligned}
B_{1j} &= -G_{\mathrm{p}}IE + G_{\mathrm{p}}v^2\rho I + Av^2EI\rho - Av^4I\rho^2 - k^*AGEI + k^*AGv^2\rho I,\\
B_{2j} &= \mathrm{i}cEIv - \mathrm{i}\rho Icv^3 - 2G_{\mathrm{p}}v\omega_jI\rho - 2Av\omega_jEI\rho + 4Av^3\omega_j\rho^2I + \mathrm{i}G_{\mathrm{p}}vc_{\mathrm{f}} - \mathrm{i}\rho c_{\mathrm{f}}v^3A\\
&\quad - 2AG\omega_j\rho Ik^* + \mathrm{i}vc_{\mathrm{f}}k^*AG,\\
B_{3j} &= -\mathrm{i}c\omega_jEI + 3Icv^2\omega_j\rho I + G_{\mathrm{p}}\omega_j^2\rho I + A\omega_j^2EI\rho - 6Av^2\omega_j^2I\rho^2 + cc_{\mathrm{f}}v^2 - \mathrm{i}G_{\mathrm{p}}\omega_jc_{\mathrm{f}}\\
&\quad + 3\mathrm{i}Av^2\omega_j\rho c_{\mathrm{f}} - EIk_1 + \rho Iv^2k_1 - G_{\mathrm{p}}k_{\mathrm{f}} + \rho Av^2k_{\mathrm{f}} - G_{\mathrm{p}}k^*AG + A^2Gv^2\rho k^*\\
&\quad + AG\omega_j^2\rho Ik^* - \mathrm{i}AG\omega_jc_{\mathrm{f}}k^* - AGk_{\mathrm{f}}k^*,\\
B_{4j} &= -3\mathrm{i}cv\omega_j^2\rho I + 4Av\omega_j^3I\rho^2 - 2cv\omega_jc_{\mathrm{f}} - 3\mathrm{i}Av\omega_1^2\rho c_{\mathrm{f}} - 2v\omega_jI\rho k_1 + \mathrm{i}vc_{\mathrm{f}}k_1 + \mathrm{i}cvk_{\mathrm{f}}\\
&\quad - 2Av\omega_j\rho k_{\mathrm{f}} + \mathrm{i}AcGvk^* - 2A^2Gv\omega_j\rho k_1,\\
B_{5j} &= -k_1k^*AG - k_1k_{\mathrm{f}} + \mathrm{i}c\omega_j^3I\rho - A\omega_j^4I\rho^2 + c\omega_j^2c_{\mathrm{f}} + \mathrm{i}A\omega_j^3\rho c_{\mathrm{f}} + \omega_j^2I\rho k_1 - \mathrm{i}\omega_jc_{\mathrm{f}}k_1\\
&\quad - \mathrm{i}c\omega_jk_{\mathrm{f}} + A\omega_j^2\rho k_{\mathrm{f}} - \mathrm{i}AcG\omega_jk^* + A^2G\omega_j^2\rho k^*,\\
B_{6j} &= -EI + \rho Iv^2,\\
B_{7j} &= -2V\omega_jI\rho + \mathrm{i}vc_{\mathrm{f}},\\
B_{8j} &= \omega_j^2I\rho - \mathrm{i}\omega_jc_{\mathrm{f}} - k_{\mathrm{f}} - k^*AG
\end{aligned}
\tag{4.128}
$$

where $j=1, 2$. The steady-state response $w(X, T)$ can be solved by the following equation based on the solutions of Eqs. (4.117), (4.126), and (4.127)

$$w(X,T) = \tilde{w}_0(\eta)\,\mathrm{e}^{i\omega T} + \tilde{w}_1(\eta)\,\mathrm{e}^{i\omega_1 T} + \tilde{w}_2(\eta)\,\mathrm{e}^{i\omega_2 T} \tag{4.129}$$

In the standard ADM, the infinite series of the decomposition for the nonlinear operator $w(u)$ is suggested as follows

$$\overline{A}_j = \sum_{n=1}^{j} c(n,j)(w_0{}^3)^{(n)} \tag{4.130}$$

It should be noted that in this scheme, the sum of the subscripts in each term of A_j are equal to j. The $c(n, j)$ are products of n components of u whose subscripts sum to j, divided by the factorial of the number of repeated subscripts. Thus

$$
\begin{aligned}
&c(1,3) = w_3,\\
&c(2,3) = w_1w_2,\\
&c(3,3) = \frac{1}{6}w_1^3
\end{aligned}
\tag{4.131}
$$

So here $\overline{A}_j$ are given as

$$
\begin{aligned}
&\overline{A}_0(\eta) = w_0^3,\\
&\overline{A}_1(\eta) = 3w_0^2w_1,\\
&\overline{A}_2(\eta) = 3w_0^2w_2 + 3w_1^2w_0,\\
&\overline{A}_3(\eta) = w_1^3 + 3w_0^2w_3 + 6w_0w_1w_2,\\
&\vdots
\end{aligned}
\tag{4.132}
$$

Compared with the procedure of the modified ADM, Eq. (4.110) and Eq. (4.111) for $j=1$ are exactly the same as Eqs. (4.117) and (4.124), while Eq. (4.110) should be

$$\begin{aligned}\left(\rho Av^2-k^*AG-G_{\mathrm{p}}\right)\tilde{w}_2''-cv\tilde{w}_2'+k_1\tilde{w}_2+k^*AG\tilde{\psi}_2'&=-3k_3\tilde{w}_0^2\tilde{w}_1\\ \left(\rho Iv^2-EI\right)\tilde{\psi}_2''-c_{\mathrm{f}}v\tilde{\psi}_2'+\left(k^*AG+k_{\mathrm{f}}\right)\tilde{\psi}_2-k^*AG\tilde{w}_2'&=0\end{aligned} \tag{4.133}$$

for $j=2$, and Eq. (4.127) should be

$$\begin{aligned}\tilde{w}_2(\eta)&=-3k_3\int_{-\infty}^{+\infty}\tilde{w}_0^2\left(\eta-\eta^*\right)\tilde{w}_1\left(\eta-\eta^*\right)\hat{w}_{21}\left(\eta^*\right)\mathrm{d}\eta^*,\\ \tilde{\psi}_2(\eta)&=-3k_3\int_{-\infty}^{+\infty}\tilde{w}_0^2\left(\eta-\eta^*\right)\tilde{w}_1\left(\eta-\eta^*\right)\hat{\psi}_{21}\left(\eta^*\right)\mathrm{d}\eta^*\end{aligned} \tag{4.134}$$

After comparing Eq. (4.125) with Eq. (4.132) and Eq. (4.127) with Eq. (4.133), one can find that the modified ADM includes more terms than the standard ADM. The extra terms cause a huge number of calculations for the steady-state response, and the calculations for the closed form solutions are more complicated.

4.4.4 The Moving Force

In this part, numerical examples are given for parametric research. The physical and geometric properties of the Timoshenko beam, the foundation and the moving load are listed in Table 4.4.

In part three, the decomposition series for the Adomian decomposition were found. But the convergence of the decomposition series has not been determined. Accordingly, let

$$\alpha_j=\begin{cases}\dfrac{\left\|w_{j+1}\right\|}{\left\|w_j\right\|},\left\|w_j\right\|\neq 0\\ 0,\left\|w_j\right\|=0\end{cases} \tag{4.135}$$

$$\left\|w_j\right\|=\max_{\eta}\mathrm{Abs}[w_j(\eta)] \tag{4.136}$$

The decomposition series Eq. (4.129) will converge rapidly to an exact solution for $0\le\alpha_j<1,\ j=0,1,2,\ldots$. According to Table 4.4 and Eqs. (4.89) and (4.135), one can obtain

$$\left\|w_0\right\|=0.000345 \tag{4.137}$$

$$\left\|w_1\right\|=0.000046454 \tag{4.138}$$

Table 4.4 Properties of the beam, foundation, and load. (Reprinted from ref. [19], with kind permission from Springer Science+Business Media)

Item	Notation	Value
Beam		
Young's modulus(steel)	E	201 GPa
Shear modulus	G	77 GPa
Mass density	ρ	7850 kg/m^3
Cross sectional area	A	7.69×10^{-3} m^2
Second moment of area	I	3.055×10^{-5} m^4
Shear coefficients	k'	0.4
Foundation		
Linear stiffness	k_1	3.5×10^7 N/m^2
Nonlinear stiffness	k_3	4×10^{14} N/m^4
Viscous damping	μ	1732.5×10^3 Ns/m^2
Shear parameter	G_p	66687500 N
Rocking stiffness	k_f	10^8 N/m^2
Rocking Damping coefficients	c_f	1.5×10^6 N·s/m^2
Moving load		
Load	F_0	65 KN
Speed	v	50 m/s

$$\|w_2\| = 0.0000294 \tag{4.139}$$

$$\alpha_0 = \frac{\|w_1\|}{\|w_0\|} \approx 0.1346 < 1 \tag{4.140}$$

$$\alpha_1 = \frac{\|w_2\|}{\|w_1\|} \approx 0.633 < 1 \tag{4.141}$$

In the following computations, the infinite decomposition series Eq. (4.105) only keeps the first three terms.

Based on the prescribed method, a computer program has been provided to solve the problem. To realize the steady–state response, it is sufficient to study the vibration of any point of the beam. Hence, the point $x=0$ is used in the following numerical examples. As the first example, the dynamic response of the infinite Timoshenko beam is considered during passage of a moving load. Figure 4.25 shows the time history of the Timoshenko beam subjected to the moving concentrated force. For $t<0$, the transverse deflection increases with time, and the largest deflection does not appear in $t=0$, but there is a little delay. After reaching the largest deflection, the transverse deflection decreases and tends toward zero while the growth speed of the transverse deflection is far greater than the reduced speed.

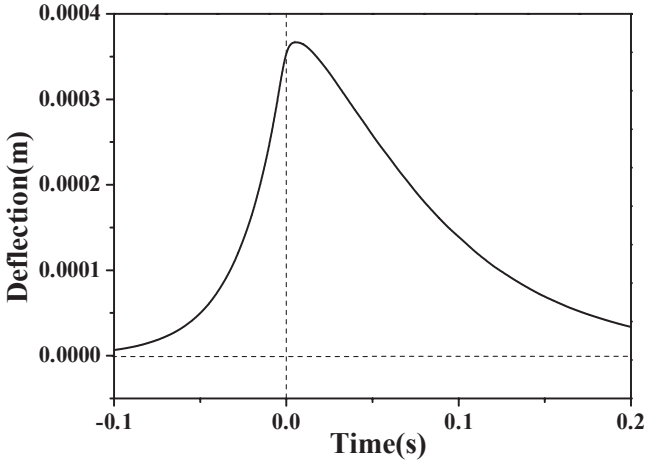

Fig. 4.25 The approximate analytical solution of the deflection of the beam. (Reprinted from ref. [19], with kind permission from Springer Science+Business Media)

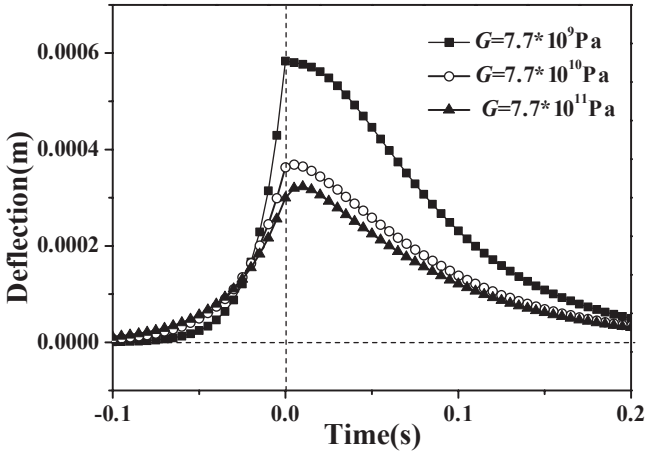

Fig. 4.26 Effect of the shear modulus of the Timoshenko beam on the deflection of the beam Timoshenko. (Reprinted from ref. [19], with kind permission from Springer Science+Business Media)

The effects of the shear modulus of the Timoshenko beam and the shear modulus of the foundation on the deflection of the beam on the viscoelastic nonlinear foundation are illustrated in Figs. 4.26 and 4.27, respectively. From the observation of Figs. 4.26 and 4.27, it is found that the largest deflection of the Timoshenko beam decreases with the increasing shear moduli of the beam and the foundation. Furthermore, Figs. 4.26 and 4.27 show that the contributions of the shear moduli of the beam and the foundation on the deflection are significant, especially when the

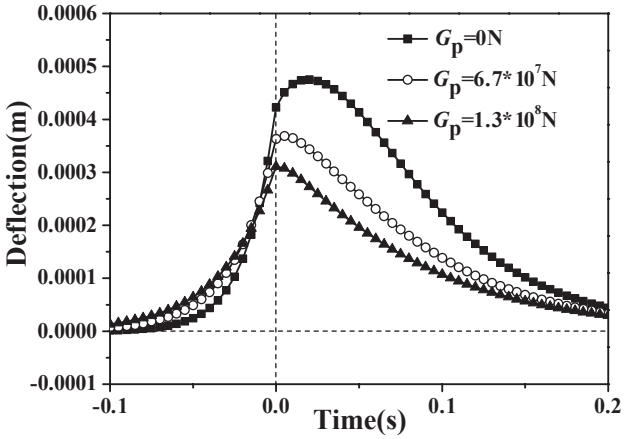

Fig. 4.27 Effect of the shear modulus of the foundation on the deflection of the beam. (Reprinted from ref. [19], with kind permission from Springer Science+Business Media)

shear moduli of the beams and the foundations are small. That is, the shear moduli of both the beams and the foundations cannot be neglected for the dynamic response of infinite beams on nonlinear viscoelastic foundations. In this section, the effects of the shear moduli of the beams and the foundations are investigated at the same time, and similar results are found at the above mentioned two references. On the other hand, the numerical results also indicate that the shear modulus of Timoshenko beams is not sensitive to the time delays of the largest deflection while the time delays decrease with the increasing shear modulus of the foundations.

Figure 4.28 shows the effect of the modulus of the elasticity of the beam on the deflection of the Timoshenko beam on the viscoelastic nonlinear foundation. As it

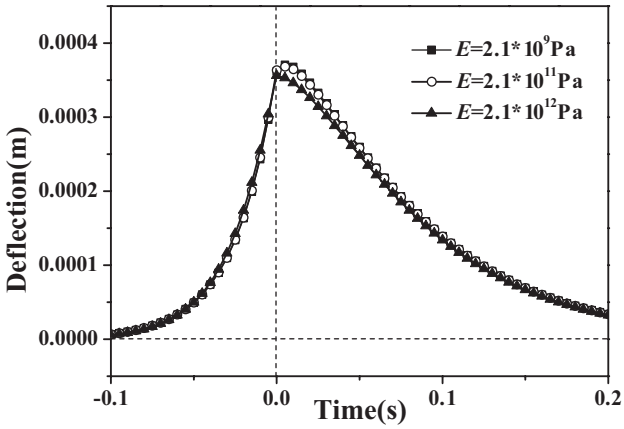

Fig. 4.28 The effect of the modulus of the elasticity of the Timoshenko beam on the deflection of the beam. (Reprinted from ref. [19], with kind permission from Springer Science+Business Media)

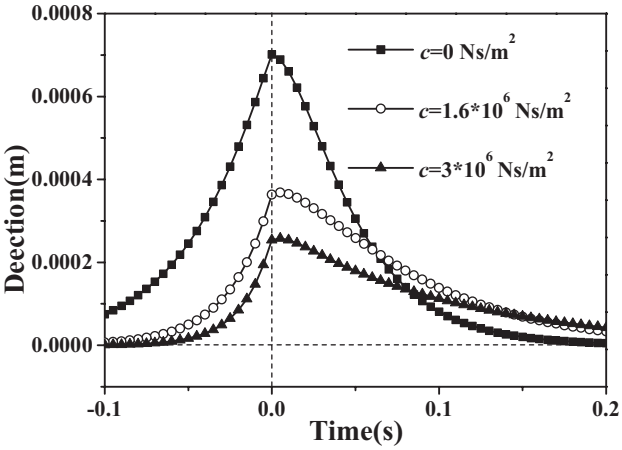

Fig. 4.29 The effect of the damping coefficient of the foundation on the deflection of the beam. (Reprinted from ref. [19], with kind permission from Springer Science+Business Media)

is seen in this figure, the modulus of the elasticity of the Timoshenko beam has little effect on the transverse deflection of the Timoshenko beam. Specifically, there are only discernible differences between the results for rather large and different modulus of the elasticity of the Timoshenko beam.

Figure 4.29 illustrates the effect of the damping coefficient of the foundation on the deflection of the Timoshenko beam on the viscoelastic nonlinear foundation. It should be noted that the viscoelastic foundation turns into an elastic Pasternak foundation when $c=0$. The numerical result shows that the damping coefficient of the foundation has significant influence on the dynamic response of the deflection of the Timoshenko beam and the deflection decreases with the increasing damping coefficient. Furthermore, the numerical result shows that the largest deflection of the Timoshenko beam on the elastic Pasternak foundation appears at $t=0$. Moreover, the time of the largest deflection appearing is delayed with the increasing damping coefficient of foundations. Hence a larger value of the damping coefficient of foundations leads to a smaller deflection of the beam and the damping is one of the reasons for the time delay.

The effects of the linear and the nonlinear elasticity parameters of the foundations on the deflection of the Timoshenko beam on the viscoelastic nonlinear foundation are displayed in Figs. 4.30 and 4.31. Figures 4.30 and 4.31 show that the form of the deflection of the beam has little change with different linear and nonlinear elasticity parameters of the foundations. Furthermore, the numerical results of Figs. 4.30 and 4.31 show that the largest deflection of the beams decreases with the increasing linear elasticity parameter of the foundation and the decreasing nonlinear elasticity parameter.

Figures 4.32 and 4.33 show that the dynamic responses of the Timoshenko beam on the viscoelastic nonlinear foundation change with the rocking stiffness and the damping coefficients of foundation. As seen in this figures, the shape has little

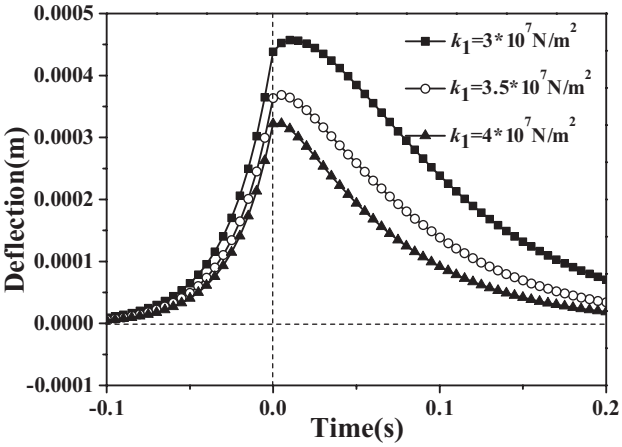

Fig. 4.30 The effect of the linear elasticity parameter of the foundation on the deflection of the beam. (Reprinted from ref. [19], with kind permission from Springer Science+Business Media)

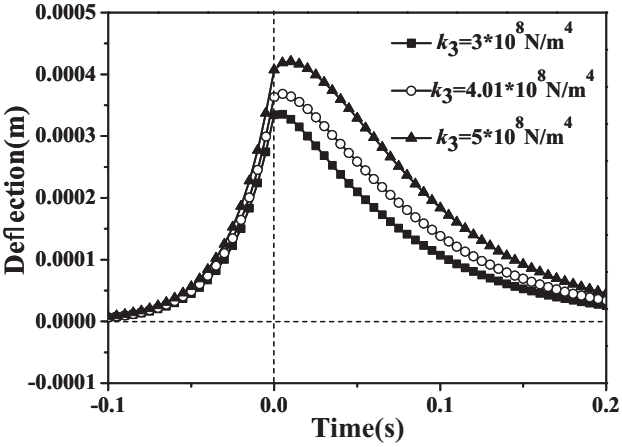

Fig. 4.31 The effect of the nonlinear elasticity parameter of the foundation on the deflection of the beam. (Reprinted from ref. [19], with kind permission from Springer Science+Business Media)

change and the largest deflection decreases with the increasing foundation rocking stiffness and damping coefficients. It proves that the influences of the rocking stiffness and damping coefficients of the foundation on the transverse deflection of the infinite beam on the foundation cannot be neglected.

The effect of the velocity of the moving concentrated force on the deflection of the Timoshenko beam on the viscoelastic nonlinear foundation is displayed in Fig. 4.34. Figure 4.34 indicates that the largest deflection of the Timoshenko beam decreases with the increasing moving velocity. Furthermore, the deflection of the beam is sensitive to the changing moving velocity. On the other hand, the numerical

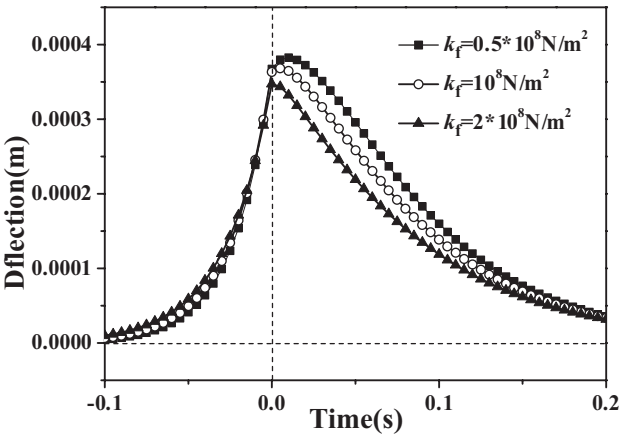

Fig. 4.32 The effect of the foundation rocking stiffness on the deflection of the beam. (Reprinted from ref. [19], with kind permission from Springer Science+Business Media)

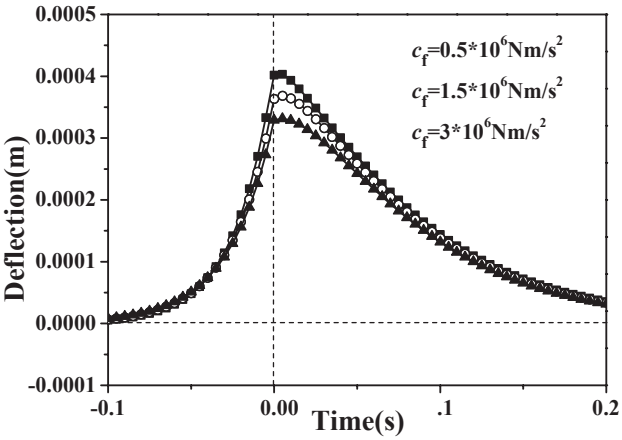

Fig. 4.33 The effect of the foundation damping coefficient on the deflection of the beam. (Reprinted from ref. [19], with kind permission from Springer Science+Business Media)

results in Fig. 4.34 prove that the whole form of the deflection of the Timoshenko beam on the viscoelastic nonlinear foundation has little change under different velocities of the moving concentrated force.

The deflections of two different beam models on the viscoelastic nonlinear foundation are compared in Fig. 4.35. As it is seen from the figure, the deflection of the Timoshenko beam near the region of $t=0$ is smaller than that of the Euler–Bernoulli beam. Furthermore, the deflection of the Timoshenko beam on the foundation is larger than that of the Euler–Bernoulli beam in other regions. Nevertheless, the Euler–Bernoulli beam is more acceptable for the dynamic response of the beam on the foundation in this investigation, because the Euler–Bernoulli beam overestimates the results of the dynamic response. In other words, the numerical results in

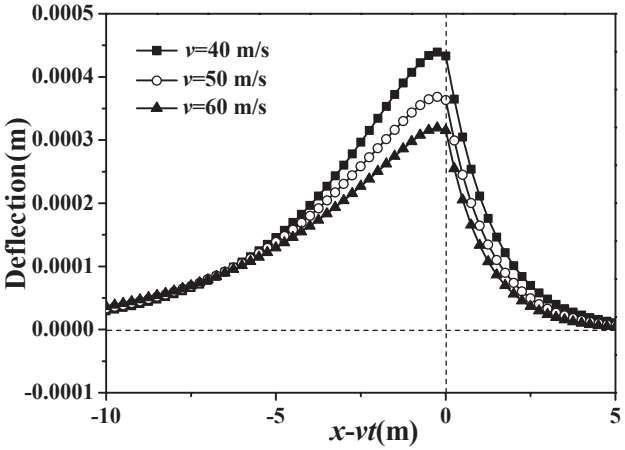

Fig. 4.34 Influence of the moving velocity of the load on the deflection of the beam. (Reprinted from ref. [19], with kind permission from Springer Science+Business Media)

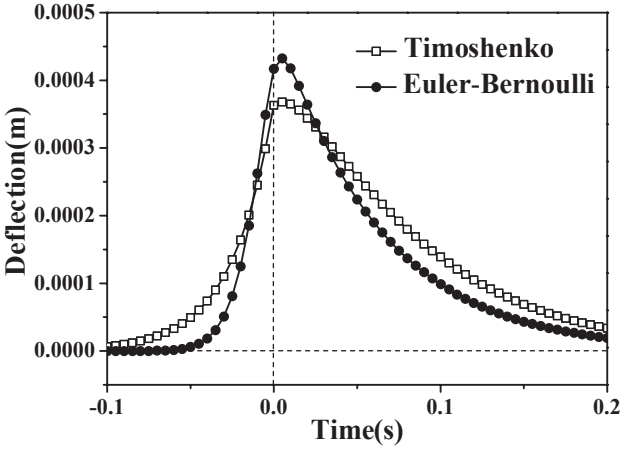

Fig. 4.35 Comparison of two different beam models from the deflection of the beam. (Reprinted from ref. [19], with kind permission from Springer Science+Business Media)

Fig. 4.35 illustrate that the dynamic response based on the Euler–Bernoulli beam theory provides a more conservative estimate in road design.

4.4.5 Parametric Studies

In this part, numerical examples are given for parametric research. The physical and geometric properties of the beam, the foundation and the moving load are listed in Table 4.4.

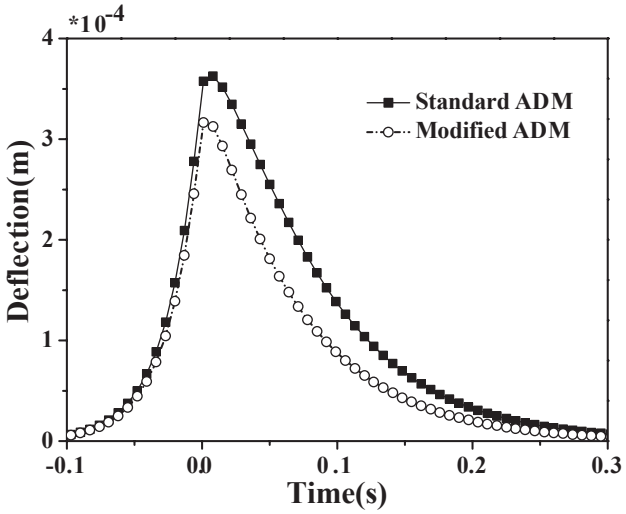

Fig. 4.36 The approximate analytic solution of deflection of the beam. (Reprinted from ref. [25], Copyright 2014, with permission from Elsevier)

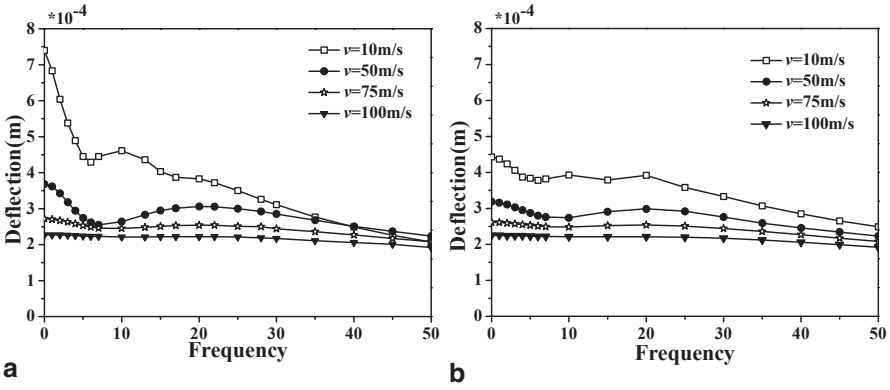

Fig. 4.37 The effects of the moving speed on the approximate analytic solution of deflection of the beams: **a** the standard ADM; **b** the modified ADM. (Reprinted from ref. [25], Copyright 2014, with permission from Elsevier)

The steady-state responses of a point at $x=0$ of the Timoshenko beam on a viscoelastic nonlinear foundation based on the modified ADM and the standard ADM are compared in Fig. 4.36. As pointed out by Wazwaz [30], the modification demonstrated a rapid convergence of the series solution if compared with the standard ADM. As it can be seen from the figure, the largest deflections of the Timoshenko beam via the modified ADM are smaller than those via the standard ADM. Although the modified ADM may give more accurate results, in the investigations of dynamic response of beams on a foundation, the standard ADM is more conservative.

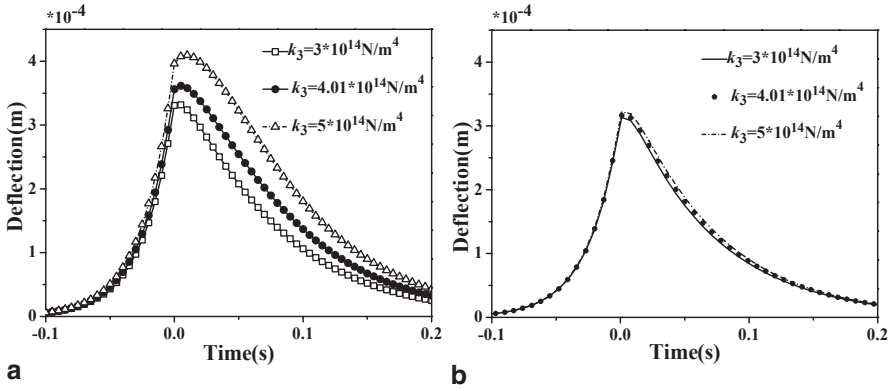

Fig. 4.38 The effects of the nonlinear elasticity parameter of foundations on the deflection of the beams: **a** the standard ADM; **b** the modified ADM. (Reprinted from ref. [25], Copyright 2014, with permission from Elsevier)

Figure 4.37 illustrates the effects of the speed of the moving load on the dynamic responses of the beam changing with the frequency of the external load. Figure 4.37a and b show the numerical results solved by the standard ADM and the modified ADM, respectively. The numerical results indicate that the largest deflection of the beams decreases with the increasing moving speed for both ADMs. Furthermore, Fig. 4.37a and b both show that the responses are more sensitive to the frequency of the external load for the smaller moving speed. The figures also demonstrate that the two kinds of ADM yield the qualitatively same results, while there are quantitative differences.

Based on the two kinds of ADMs, the effects of the nonlinear elasticity parameter of the foundations on the deflection of the infinite beams on a nonlinear foundation are displayed in Fig. 4.38a and b, respectively. Figure 4.38 shows that the shapes of the time history of the Timoshenko beam center are almost the same for different nonlinear parameters of the foundation. Moreover, the numerical results of Fig. 4.38 show that the largest deflections of the beams increase with the increasing nonlinear elasticity parameter of the foundation. The numerical results also indicate that the results from the two ADMs qualitatively predict the same tendencies with the changing parameters, while quantitatively there are certain differences. The results via the standard ADM are more sensitive to nonlinear parameters than those via the modified ADM.

The effects of the shear modulus of the foundation, the shear modulus of Timoshenko beams and the rocking damping coefficients on the deflection of the infinite Timoshenko beams on a nonlinear viscoelastic Pasternak foundation with $v=50$ m/s and $\omega=1$ Hz are shown in Figs. 4.39, 4.40 and 4.41, respectively. The numerical results show that the largest deflections of beams decrease with the shear modulus of the beam, the shear modulus of the foundation and the rocking damping coefficient, and the shear moduli of the beams and the foundation cannot be neglected. The numerical simulations also indicate results via the standard ADM are more sensitive to shear modulus parameters than those via the modified ADM.

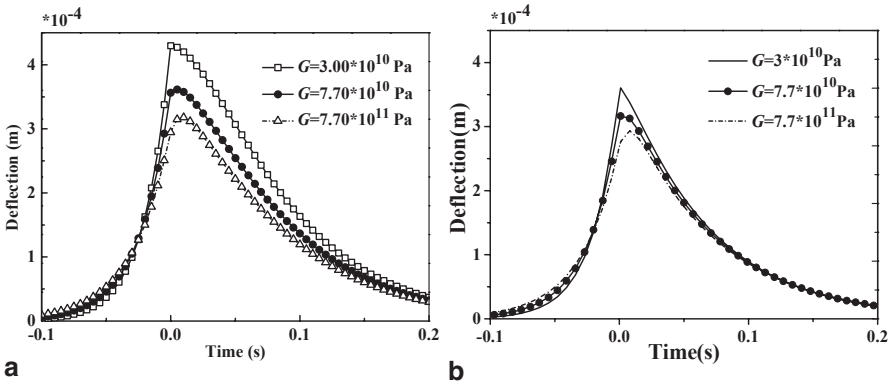

Fig. 4.39 The effects of the shear modulus of beams on the deflection of the beams: **a** the standard ADM; **b** the modified ADM. (Reprinted from ref. [25], Copyright 2014, with permission from Elsevier)

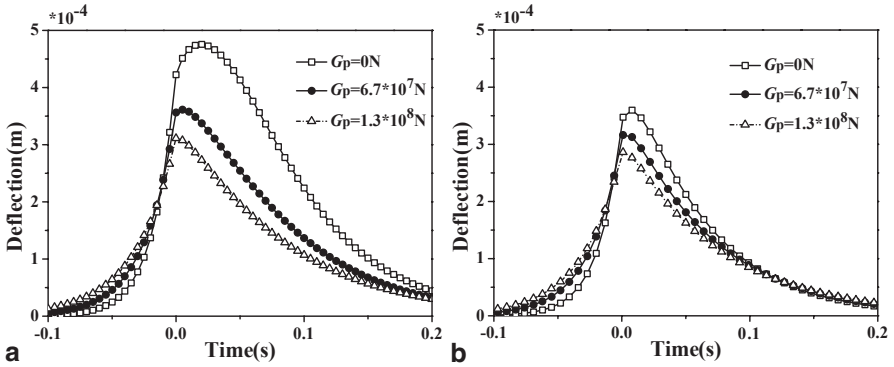

Fig. 4.40 The effects of the shear modulus of foundations on the deflection of the beams: **a** the standard ADM; **b** the modified ADM. (Reprinted from ref. [25], Copyright 2014, with permission from Elsevier)

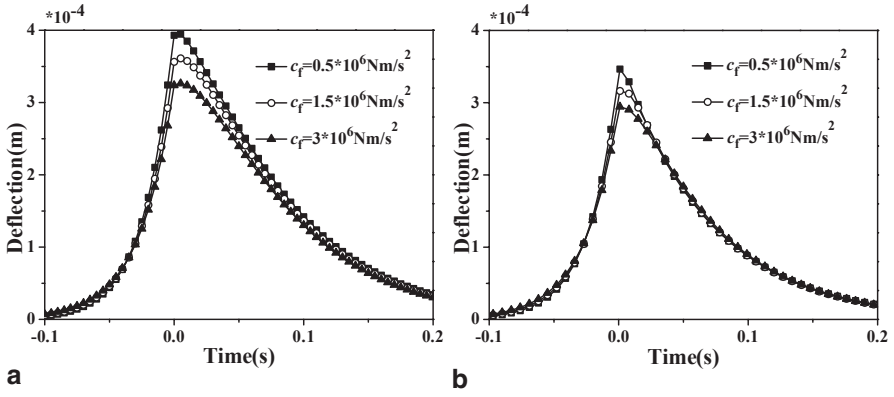

Fig. 4.41 The effects of the rocking damping coefficients on the deflection of the beams: **a** the standard ADM; **b** the modified ADM. (Reprinted from ref. [25], Copyright 2014, with permission from Elsevier)

4.5 Chapter Summary

This chapter is devoted to the dynamic analysis of a pavement structure under a vehicle's moving load. The pavement structure is modeled as a finite Euler–Bernoulli beam on a nonlinear foundation, a finite Timoshenko beam on a nonlinear Pasternak foundation and an infinite Timoshenko beam on a nonlinear foundation with viscous damping. Moreover, three types of the conventional boundary conditions, namely SS, CC, and FF boundary conditions are investigated. The numerical simulation found that the vertical deflections of the pavement for three boundary conditions are overlapped with a rather large length of the pavement. The vehicle's moving load is considered as a moving concentrated load, a harmonic moving load and a moving spring-mass-damper oscillator, respectively.

Based on the dynamic response of the pavement-vehicle system, the convergence of the Galerkin truncation and the dependences on the system parameters are numerically studied. It was found that the convergence of the Galerkin truncation can be predicted by the natural frequencies, the slow growth in the natural frequency of the pavement causes lack of convergence, and investigation into dynamical responses of the vehicle–pavement-foundation system needs large truncation terms. Furthermore, the convergence increases with growing of the moduli of elasticity of the pavement and the nonlinear foundation parameters but decrease with the increasing linear foundation parameters and the damping coefficient. Moreover, the convergence of the Galerkin truncation for Timoshenko beams on foundations is slightly slower than that of the Euler–Bernoulli beam. Nevertheless, the vertical deflections of the Timoshenko beam are slightly larger.

To account for shear deformations of the pavement and the subgrade, the shear modulus of the beam and the shear deformation coefficient of the foundation are considered at the same time. Therefore, nonlinear coupled dynamics of the vehicle–pavement system is investigated with a Timoshenko beam on a linear-plus-cubic Pasternak-type foundation under a moving spring-mass-damper oscillator. The numerical examples revealed that the amplitude of the vibratory responses of the pavement becomes smaller when the vehicle is close to resonance.

In conjunction with complex Fourier transformation, the ADM and a perturbation method are, respectively, used to deal with the nonlinear term from the foundation reaction for the dynamic analysis of infinite Timoshenko beams on the nonlinear foundation. This chapter proves that the ADM and the perturbation method give the consistent result for current issues.

References

1. Li SH, Yang SP, Xu BQ, Xing HJ. Chaos of a beam on a nonlinear elastic foundation under moving loads. 2007 International Symposium on Nonlinear Dynamics. J Phys Conf Ser. 2008;96(1):012116.
2. Sheng DF, Zhang Y, Cheng CJ. Dynamic behavior of nonlinear viscoelastic Timoshenko beams with damage on a viscoelastic foundation. J Shanghai Univ (English Edition). 2004;8(3):245–51.

3. Pellicano F, Mastroddi F. Nonlinear dynamics of a beam on an elastic foundation. Nonlinear Dyn. 1997;14(4):335–55.
4. Ansari M, Esmailzadeh E, Younesian D. Internal-external resonance of beams on a non-linear viscoelastic foundation traversed by a moving load. Nonlinear Dyn. 2010;61(1–2):163–82.
5. Ansari M, Esmailzadeh E, Younesian D. Frequency analysis of finite beams on a nonlinear Kelvin–Voight foundation under moving loads. J Sound Vib. 2011;330(7):1455–71.
6. Yan T, Kitipornchai S, Yang J. Dynamic behavior of edge-cracked shear deformable functionally graded beams on an elastic foundation under a moving load. Compos Struct. 2011;93(11):2992–3001.
7. Coskun I. Non-linear vibrations of a beam on a tensionless Winkler foundation. J Sound Vib. 2000;236(3):401–11.
8. Celep Z, Güler K, Demir F. Response of a completely free beam on a tensionless Pasternak foundation subjected to dynamic load. Struct Eng Mech. 2011;37(1):61–77.
9. Vassilev VM, Djondjorov PA. Dynamic stability of viscoelastic pipes on elastic foundations of variable modulus. J Sound Vib. 2006;297(1–2):414–9.
10. Yang SP, Li SH, Lu YJ. Investigation on dynamic interaction between a heavy vehicle and road pavement. Veh Syst Dyn. 2010;48(8):923–44.
11. Chen JS, Chen YK. Steady state and stability of a beam on a damped tensionless foundation under a moving load. Int J Non-Linear Mech. 2011;46(1):180–5.
12. Senalp AD, Arikoglu A, Ozkol I. Dynamic response of a finite length Euler–Bernoulli beam on linear and nonlinear viscoelastic foundations to a concentrated moving force. J Mech Sci Technol. 2010;24(10):1957–61.
13. Thambiratnam D, Zhuge Y. Dynamic analysis of beams on an elastic foundation subjected to moving loads. J Sound Vib. 1996;198(2):149–69.
14. Muscolino G, Palmeri A. Response of beams on viscoelastically damped foundation to moving oscillators. Int J Solids Struct. 2007;44(5):1317–36.
15. Arboleda-Monsalve LG, Zapata-Medina DG, Aristizabal-Ochoa JD. Timoshenko beam-column with generalized end conditions on an elastic foundation: dynamic-stiffness matrix and load vector. J Sound Vib. 2008;310(4–5):1057–79.
16. Ding H, Chen LQ, Yang SP. Convergence of Galerkin truncation for dynamic response of finite beams on nonlinear foundations under a moving load. J Sound Vib. 2012;331(10):2426–42.
17. Contreras JN, Castro-Fresno D, Vega-Zamanillo A. Dynamic modulus of an asphalt mixture by ultrasonic direct test. NDT E Int. 2010;43(7):629–34.
18. Yang Y, Ding H, Chen LQ. Dynamic response to a moving load of a Timoshenko beam on a nonlinear viscoelastic foundation. Acta Mech Sin. 2013;29(5):718–27.
19. Ding H, Shi KL, Chen LQ, Yang SP. Dynamic response of an infinite Timoshenko beam on a nonlinear viscoelastic foundation. Nonlinear Dyn. 2013;73:285–98.
20. Cao CY, Zhong Y. Dynamic response of a beam on a Pasternak foundation under a moving load. J Chongqing Univ. 2008;7:311–6.
21. Ding H, Yang Y, Chen LQ, Yang SP. Vibration of vehicle–pavement coupled system based on a Timoshenko beam on a nonlinear foundation. J Sound Vib. 2014;333(24):6623–36.
22. Bhattiprolu U, Bajaj AK, Davies P. An efficient solution methodology to study the response of a beam on a viscoelastic and nonlinear unilateral foundation: static response. Int J Solids Struct. 2013;50:2328–39.
23. Palmeri A, Cicirello A. Physically-based Dirac's delta functions in the static analysis of multi-cracked Euler–Bernoulli and Timoshenko beams. Int J Solids Struct. 2011;48:2184–95.
24. Thambiratnam D, Zhuge Y. Dynamic analysis of beams on an elastic foundation subjected to moving loads. J Sound Vib. 1996;198:149–69.
25. Ding H, Shi KL, Chen LQ, Yang SP. Adomian polynomials for nonlinear response of supported Timoshenko beams subjected to a moving harmonic load. Acta Mech Solida Sin. 2014;27(4):383–93.
26. Kargarnovin MH, Younesian D, Thompson DJ. Response of beams on nonlinear viscoelastic foundations to harmonic moving loads. Comput Struct. 2005;83(23–24):1865–77.

27. Hryniewicz Z. Dynamics of a Rayleigh beam on a nonlinear foundation due to a moving load using Adomian decomposition and coiflet expansion. Soil Dyn Earthq Eng. 2011;31(8):1123–31.
28. Adomian G. A new approach to nonlinear partial differential equations. J Math Anal Appl. 1984;102(2):420–34.
29. Vahidi AR, Jalalvand B. Improving the accuracy of the Adomian decomposition method for solving nonlinear equations. Appl Math Sci. 2012;6(10):487–97.
30. Wazwaz AM. A reliable modification of the Adomian decomposition method. Appl Math Comput. 1999;102(1):77–86.